AD-755 947

SYNTHESIS OF COMPOUND SEMICONDUCTING MATERIALS AND DEVICE APPLICATIONS

D. A. Stevenson

Stanford University

Prepared for:

Advanced Research Projects Agency

31 December 1972

DISTRIBUTED BY:

NTIS

National Technical Information Service
U. S. DEPARTMENT OF COMMERCE
5285 Port Royal Road, Springfield Va. 22151

BEST
AVAILABLE COPY

AD755947

SEMI-ANNUAL TECHNICAL REPORT

SYNTHESIS OF COMPOUND SEMICONDUCTING MATERIALS AND DEVICE APPLICATIONS

July 1, 1972 - December 31, 1972

Reproduced by
NATIONAL TECHNICAL
INFORMATION SERVICE
U S Department of Commerce
Springfield VA 22151

Grant No. DAHC15 72-G-6

D D C
RECEIVED
FEB 27 1973
B

This document has been approved for public release and sale; its distribution is unlimited.

The views and conclusions contained in this document are those of the authors and should not be interpreted as necessarily representing the official policies, either expressed or implied, of the Advanced Research Projects Agency or the U. S. Government.

CMR-73-2

CENTER FOR MATERIALS RESEARCH

STANFORD UNIVERSITY • STANFORD, CALIFORNIA

Semi-Annual Technical Report

July 1, 1972 - December 31, 1972

Sponsored by
Advanced Research Projects Agency
ARPA Order No. 1644-2

Program Code Number: POD10

Contractor: Stanford University

Grant No. DAHC15 72-G-6

Principal Investigator: D. A. Stevenson
Phone: (415) 321-2300, Ext. 4251

Co-Investigators:
R. H. Bube, Ext. 2535
R. S. Feigelson, Ext. 4007
G. S. Kino, Ext. 72289
B. L. Mattes, Ext. 2695
W. D. Nix, Ext. 4259
R. K. Route, Ext. 2695
W. A. Tiller, Ext. 2301

Effective Date of Grant: July 1, 1972

Grant Expiration Date: June 30, 1973

Amount of Grant: $193,350

Grant Title: Synthesis of Compound Semiconducting Materials and Device Applications

Center for Materials Research
Stanford University
Stanford, California 94305
(415) 321-2300, Ext. 4118

CMR 73-2

TABLE OF CONTENTS

I.	INTRODUCTION	1
II.	EPITAXIAL CRYSTAL GROWTH	3
III.	APPLICATIONS OF COMPOUND SEMICONDUCTOR MATERIALS	11
IV.	RELATIONS BETWEEN DISLOCATIONS AND MECHANICAL PROPERTIES AND THE PRODUCTION AND CHARACTERIZATION OF DEFECT STRUCTURES IN COMPOUND SEMICONDUCTORS	14
V.	SCIENTIFIC ASPECTS OF GALLIUM ARSENIDE CRYSTAL PREPARATION	25
VI.	VAPOR PHASE GROWTH OF GaN ELECTROLUMINESCENT DIODES	28

I. INTRODUCTION

The present program concerns the synthesis of compound semiconducting materials, with particular emphasis on their use in new and novel microwave devices. The program is divided into three major sections: thin film epitaxial growth of III-V compounds; the design, fabrication and evaluation of microwave devices and fundamental studies of crystal synthesis and properties.

The devices of primary interest are of the planar microwave and acoustical type, employing thin films of GaAs as the active layer. The choice of GaAs was made based on its unique properties: exceptionally high carrier mobility, a moderately large band gap, the Gunn effect and piezoelectric response. These planar devices require high quality active layers of GaAs, with particularly strict requirements on film thickness, surface smoothness, carrier density, and mobility in the film. The layers intended for microwave devices are grown by the liquid phase epitaxial technique.

In the period covered by this report, there has been significant activity on all aspects of the program. The major activity of the epitaxial crystal growth section of the program has been the study of mechanisms for contamination of layers during growth. It had been noted that some layers had deteriorated in quality concurrent with improvements made in the growth procedure. A major consideration in elucidating this behavior has been the interaction of the graphite crucibles, the quartz containers and the high purity hydrogen protective atmosphere, with particular reference to possible chemical vapor transport of impurities. In the device fabrication segment of the program, several travelling wave

amplifiers were produced using material from various sources. Difficulties were encountered in making ohmic contacts to the very thin layers that were necessitated by modifications in the device design. The basic study of the defect structure of GaAs has concentrated on the understanding of the photoconductivity characteristics of high resistivity GaAs, namely, GaAs:Cr, and GaAs:O. A larger number of imperfection levels were noted in these materials. In the study of the scientific aspects of GaAs crystal preparation, there have been refinements in the theoretical calculations of the structure and energetics of the GaAs(S) - Ga(L) interfaces. The treatment has been refined to produce more satisfactory results. In the vapor growth of GaN, rather exciting results have been obtained. A materials growth and device fabrication procedure has been developed that produces violet electroluminescence. To the best of our knowledge, this is the first such device to produce light at this wavelength. A description of these respective activities is given below.

II. EPITAXIAL CRYSTAL GROWTH

R. S. Feigelson, B. L. Mattes, R. K. Route and P. Pettit

A. PROGRAM OBJECTIVE

The principal objective of the epitaxial growth program is the preparation of high quality, uniform and reproducible epitaxial layers of GaAs for the device applications program. The device program requires layers (not obtainable commercially) that have carrier densities in the low 10^{14} cm^{-3} to 10^{15} cm^{-3} range, 300°/77°K mobilities above 7000/50,000 cm^2/V-sec, thicknesses in the .5-30μm range, and optically smooth surfaces.

In order to meet this objective, considerable effort has been devoted to the development of new methods of growth, the study of variables that influence growth, techniques to prepare and handle materials involved in growth, and methods to evaluate the growth and its properties. In addition, the epitaxial crystal growth program is coordinated with the materials studies and device applications programs to prepare materials with specific properties and dimensions and to interact on problems of mutual concern.

The most recent objective in this program is the reduction of background impurity levels to improve the quality and reproducibility of the electrical properties of the epitaxial layers. The results from reactions observed between high purity hydrogen on carbon and fused quartz has prompted a study on less reactive materials in the system, e.g., argon, Al_2O_3 ceramics and pyrolytic BN.

The future objectives of the epitaxial crystal growth program will be: (1) to meet the device application and materials study program

requirements for III-V materials with specific properties; (2) to continue the development and evaluation of ohmic contacts on GaAs epitaxial layers; (3) to continue the analysis of the liquid phase growth process, in particular, nucleation phenomena and the incorporation of impurities; and (4) to develop techniques for growing epitaxial GaAs on oxide substrates.

B. PROGRESS

1. Achievements

The liquid phase epitaxial growth systems have been modified to eliminate sources of contamination that may arise from gas leaks and questionable materials. These modifications include glass to metal seals in place of viton O-ring seals, stainless steel gland fittings with nickel gaskets and He-arc welds in place of Swagelok fittings, and new quartz reactor tubes and purified graphite boats. These changes have improved the reproducibility of electrical properties of the layers, but the electrical properties have not been appreciably improved. Under ultra tight and contamination free conditions there appears to be a graphite-fused quartz reaction above 600°C that degrades the electrical properties of the layers. Changes are presently in progress to circumvent this problem by studying the effects of growth and bakeout temperatures, high purity ceramic Al_2O_3, pyrolytic BN, and purified Ar on the electrical properties of the layers.

2. Growth Studies

Improvements have been made to eliminate leaks and questionable material contaminations in the growth system. Unforeseen difficulties,

however, have arisen from these changes--the electrical quality of the layers has decreased yielding $4x10^{15}$ to $4x10^{16}$ cm^{-3} carrier densities and 4500-6500/10,000-30,000 cm^2/V-sec mobilities at 300°/77°K. On the other hand, the reproducibility and uniformity of the electrical properties have improved. The layers are heavily contaminated with carbon and oxygen, as determined from mass spectrometric analyses. Photoluminescence measurements have indicated the presence of silicon as a major impurity. The impurities, carbon, oxygen and silicon, appear to be associated with reactions between the graphite growth cell, dry high purity H_2, and the fused quartz reactor tube. The Ga and/or GaAs may also take part in these reactions. However, at the growth temperatures around 700°C, without the latter, carbon and/or silicon are deposited around the graphite boat and in cooler parts of the system.

Over 100 GaAs layers were grown during the past six month period. The source of the impurities, however, has not been ascertained. Two systems, composed of a quartz reactor, graphite cell and H_2, were systematically changed and varied, but the cause has not been localized. Cleaning procedures, growth and bakeout temperatures, graphite cells, hydrogen purifiers, sources of Ga, GaAs source, GaAs substrates, etc., have all been modified but to no avail. Typical results from a series of four growths, associated with a specific change in the growth system, is shown in Table II-1. In this case, the graphite cell was vacuum fired at 1500°C, the reactor was fired at 1000°C with O_2, and then the cell and reactor were fired together at 700°C with purified H_2. New Ga and GaAs source materials were added to the system for a bakeout at 700°C under H_2. The series of growths that followed had a saturation temperature of 700°C. The principal characteristic of every series attempted was

that the second or third growths had the highest mobilities and the lowest carrier densities. There were no continuous trends to successively better results. However, by increasing the saturation temperature, e.g., to 800°C, the electrical properties will improve and appear to have the same degree of electrical compensation. This effect is now under further investigation. Long term, high temperature bakeouts above 700°C in between growths, however, severely degrade the electrical properties.

No improvements in the electrical properties were noted when the following modifications were made to the materials used or to the system: high density graphite or pyrolytic graphite, new and purified by the manufacturer or used and purified at our facilities; new or old H_2 purifiers from different manufacturers, He-leak checked to better than 10^{-12} atm-cc/sec; new or old fused quartz reactor tubes, carefully cleaned, flame polished or not; and glass to metal seals, He-arc welds and gland fittings with Ni gaskets or viton O-ring seals and stainless steel swage fittings at every joint in the system, He-leak checked to better than 10^{-12} atm-cc/sec.

By the process of elimination of various changes in the growth system, several factors in our systems remain unresolved:

(1) reduction of fused quartz by extremely dry pure H_2,

$$SiO_{2(s)} + H_{2(g)} \rightarrow SiO_{(g)} + H_2O_{(g)} ,$$

and/or

$$SiO_{2(g)} + 2H_{2(g)} \rightarrow Si_{(s)} + 2H_2O_{(g)} ;$$

(2) reduction of quartz by graphite

$$C_{(s)} + SiO_{2_{(s)}} \rightarrow CO_{(g)} + SiO_{(g)}$$

and/or

$$C_{(s)} + SiO_{2_{(s)}} \rightarrow CO_{2_{(g)}} + Si_{(s)} \; ;$$

and (3) reactions that combine (1) and/or (2) with Ga

$$Ga_{(\ell)} + 2H_2O_{(g)} \rightarrow Ga_2O_{(s)} + 2H_{2_{(g)}}$$

and/or

$$2Ga_{(\ell)} + CO_{(g)} \rightarrow Ga_2O_{(s)} + C_{(s)}$$

and/or

$$2Ga_{(\ell)} + SiO_{(g)} \rightarrow Ga_2O_{(s)} + Si_{(s)} \; .$$

Some of these reactions are normally not considered energetically possible based on thermo-equilibrium calculations. However, they might occur if (a) under extremely pure conditions some form of surface catalysis takes place or (b) there are some residual oxides present to setup a cyclic process that will introduce C, O and Si onto the epitaxial growths.

A conceivable sequence of reactions that might take place, without Ga or GaAs, is the following: (1) loosely bound SiO_2 on the walls of the fused quartz reactor tube is reduced by H_2,

$$H_{2_{(g)}} + SiO_{2_{(s)}} \rightarrow SiO_{(g)} + H_2O_{(g)} \; , \qquad (1)$$

creating water vapor; (2) the water vapor reacts with the carbon,

$$H_2O_{(g)} + C_{(s)} \rightarrow CO_{(g)} + H_{2_{(g)}} , \qquad (2)$$

creating carbon monoxide; (3) the carbon monoxide reacts with the silicon monoxide of reaction (1),

$$CO_{(g)} + SiO_{(g)} \rightarrow CO_{2_{(g)}} + Si_{(s)} , \qquad (3)$$

creating silicon which will condense in cooler portions of the reactor; and (4) the reaction becomes cyclic when the CO_2 from reaction (3) reacts with the carbon,

$$CO_{2_{(g)}} + C_{(s)} \rightarrow 2CO_{(g)} , \qquad (4)$$

creating CO which will in turn react with SiO from reaction (1). This cyclic process will not appreciably deplete the carbon source. The fused quartz, on the other hand, will only be chemically attacked until the loosely bound SiO_2 is depleted. Thus this sequence of reactions should only exhibit a finite reaction period. This process may have occurred when a highly flame polished fused quartz reactor tube was baked out with a pyrolytic graphite boat at 800°C. After 10 hours a heavy black deposit, apparently silicon, condensed onto cooler regions of the reactor, principally around the quartz spade supporting the graphite cell. The deposit decreased with further baking and disappeared completely when Ga was introduced into the graphite cell. The subsequent growths had carrier densities in the 10^{16} cm^{-3} range and very low mobilities.

A carbon reaction in the growth system is also indicated by two additional experimental observations: (1) When an all quartz system is used, i.e., the graphite cell replaced by a fused quartz cell, the

electrically active compensation changes and the carrier densities are in the low 10^{15} cm^{-3} range; and (2) when the GaAs source and two successive growths were analyzed by mass spectrometry, Table II-2, the carbon content increased 3X and the oxygen decreased 3X, paralleling the increase in carrier density, 7.2×10^{15} to 3.4×10^{16} cm^{-3}, while the total impurity content decreased only 20%. The impurity content, however, may be misleading in that part of the content included the substrate--the layers were only 10μm thick. A photoluminescence spectrum showed a massive Si peak in growth 435 compared to 434. Thus the analysis in Table II-2 may correspond principally to the impurity content in the Cr doped semi-insulating substrate.

C. PROPOSED FUTURE WORK

The principal objective for the remainder of this contract will be to solve the impurity problem so that reproducible high electrical quality layers can be obtained. Several changes in the growth systems are already underway: (1) use of pyrolytic BN, Al_2O_3 and SiO_2 growth cells; (2) replacement of the fused quartz reactor tube with a high purity ceramic Al_2O_3 tube; (3) use of purified Ar in place of purified H_2; and (4) use of an O_2 analyzer to monitor the output of the reactor. Both Al_2O_3 and BN are more stable to Ga and GaAs, and Ar should reduce the reduction of fused quartz. The purity of these new materials is in question, however, their stability may provide a key advantage. An O_2 analyzer has been designed, and the parts and equipment are available. This should be extremely useful for the evaluation of the growth reactions. Further, mass spectrographic analyses will also be made to identify the reacting species.

Since some of the present GaAs growths still meet specific property and dimensional requirements for the device program, the growth program will maintain a flexible capability to meet these commitments. Improved materials will also be made immediately available to this program.

A continued effort will be made to (1) develop n^+ layers for electrical contacts; (2) study the variables that control growth in the liquid phase process; and if time permits (3) develop heteroepitaxial techniques to grow epitaxial GaAs layers on Al_2O_3 and BeO substrates.

TABLE II-1

Electrical Properties at 300°/77°K

Growth No.	Mobility (cm^2/V-sec)	Carrier Density (cm^{-3})
465	4900/17,700	$9.7/6.4 \times 10^{15}$
466	6110/32,100	$2.6/2.1 \times 10^{15}$
467	6090/23,900	$7.4/5.6 \times 10^{15}$
468	4600/15,000	$14/9.7 \times 10^{15}$

TABLE II-1

Electrical Properties at 300°/77°K

Growth No.	Mobility (cm^2/V-sec)	Carrier Density (cm^{-3})
465	4900/17,700	$9.7/6.4 \times 10^{15}$
466	6110/32,100	$2.6/2.1 \times 10^{15}$
467	6090/23,900	$7.4/5.6 \times 10^{15}$
468	4600/15,000	$14/9.7 \times 10^{15}$

TABLE II-2

Bell & Howell Mass Spectrometric Analysis of GaAs

Element*	GaAs Source	Growth #434**	Growth #435**
	(parts per million atomic)		
B	.18	1.0	.3
C	6.4	9.8	32.
N	1.5	1 6	5.1
O	9.0	80.	26.
F	.50	1.2	1.8
Al	.76	2.5	3.6
Si	.97	3.1	4.8
Pb	.90	N.D.	N.D.
S	.98	1.5	3.0
Cl	.70	1.5	1.0
K	2.7	1.1	3.2
Ca	.28	1.2	N.D.
Cr	.22	2.1	2.6
Fe	.60	1.3	1.2
	26.0	107.9	84.6

* GaAs spectrum interferes with Na lines

** Electrical properties at 300°/77°K

# 434	6510/22,900 (cm^2/V-sec)	7.2/5.5x10^{15}(cm^{-3})
# 435	4420/12,200 (cm^2/V-sec)	3.2/1.9x10^{16}(cm^{-3})

III. APPLICATIONS OF COMPOUND SEMICONDUCTOR MATERIALS

G. S. Kino, S. Kofol and R. Bisio

A first batch of GaAs traveling wave amplifiers with Schottky-barrier input gates was designed and fabricated; their configuration and the fabrication sequence were illustrated in the previous report. A typical I-V characteristic of the devices is shown in Fig. 1. Incoherent oscillations were present at voltages slightly higher than the threshold voltages. All of the devices were tested from 2 to 10 GHz with the circuit shown in Fig. 2. All devices tended to oscillate. The capacitive coupling from input to output was relatively large due to poor shielding, so that the input-output loss of the device with no drift field applied was only of the order of 13 dB. However, although we would observe a change in output level of a few dBs at 7.5 GHz when the drift field was raised above threshold, it appeared that the coupling of the input signal into the device was extremely weak, and that changes in the external circuit had very little effect on the broadband oscillations present in the 7-12 GHz range.

A new design of the amplifier was then carried out. The main features of the new design are: reduced epi-layer thickness of 1-4 μm; a reduced value of the nd product to 1-3 x $10^{11} cm^{-2}$; input and output Schottky-barrier gates; Schottky-barrier ohmic contact extensions to control the dc field distribution; and mesa etching around the active device, so that bigger input and output gate bonding pads could be placed on the semi-insulating substrate and yet have a small capacitance to ground. A drawing of the new design is shown in Fig. 3. The thickness of the SiO_2 layer is 3000-6000 Å. The width of the device is 500-100 μm

and the other dimensions are shown in the blow-up of Fig. 4 for two different sets of devices.

The mesa etching procedure was first investigated using a (111)B orientation. We were able to obtain reasonable slopes for the mesa profile, as shown in Fig. 5, so that the gate metallization did not suffer cracks crossing the mesa step. The (100) orientation was also investigated since it is easier to obtain material with this orientation. In this case, he mesa profile depends strongly on the orientation of the mesa step on the (100) face. Reasonable slopes were obtained for mesa oriented along the $(01\bar{1})$ axis.

The construction of these devices has been delayed severely owing to difficulty in obtaining the required epitaxial material. Moreover, we have been experiencing difficulties with the process for making ohmic contacts, which had worked perfectly with all our previous material.

A first attempt was made using material provided by the Center of Material Research: CMR-283-TG, (111)B, thickness 0.8 μm, carrier density 2×10^{15} cm^{-3}, and CMR-291-TG, (111)B, thickness 2.8 μm, carrier concentration 1×10^{15}. The Ag-In-Ge contacts did not work for these two samples. We checked out procedure for making ohmic contacts processing simultaneously these two samples together with some other samples from CMR, Fairchild, and Monsanto. Ohmic contacts could be made perfectly to all the samples but CMR-283-TG and CMR-291-TG.

A second attempt was made using material purchased from Varian Associates: Varian N-44-A, (111)B, thickness 1.76 μm, carrier density 1.5×10^{15} cm^{-3}. In this case it was again not possible to make good ohmic contacts. Several attempts were made using different mathods of evaporation and alloying. The problem proved to be extremely elusive,

since we were still successful in our trials with thicker layers but could not make ohmic contacts to the thinner materials.

A third attempt was made with another sample bought from Varian Associates: Varian N-86-A, (100), thickness 2.5 μm then reduced to 1.5 um by chemical etch, carrier density 2.4×10^{15} cm^{-3}. This time the ohmic contacts were deposited at Varian Associates, and at Hawlett-Packard. The alloys used were the same, Au-Ge, but the procedures were quite different. The contacts were still not ohmic; thay were sensitive to light and showed premature current saturation. An analysis of the I-V curves vs. temperature seemed to indicata that an unusually high concentration of traps at the intarfaca batween the apitaxial layer and the semi-insulating substrate could be responsible for tha difficulties encountered in making ohmic contacts, the affact of the traps being relatively more important in thin apitaxial layars.

We are now making new attampts to construct a davice from a thicker epitaxial layer.

FIGURE CAPTIONS

Figure III-1. I-V characteristic of the GaAs amplifier, taken between source and drain, with the input Schottky-barrier gate floating.

Figure III-2. RF testing circuit for the GaAs amplifier.

Figure III-3. Schematic view of the GaAs amplifier with Schottky-barrier input and output gates. (A) semi-insulating GaAs substrate; (B)n-type GaAs epitaxial layer;(C) ohmic contacts;(D_1) Schottky-barrier contact extension;(D_2)Schottky-barrier gates;(E) insulating layer;(F) insulated gate.

Figure III-4. Blow-up of the center section of the amplifier.

	I (μm)	II (μm)
ℓ_1	93	70
ℓ_2	85	65
ℓ_3	5	5
ℓ_4	5	5
ℓ_5	65	45
ℓ_6	56	36

Figure III-5. Mesa profile on the <111>B face. Mesa step is 3.8 μm; etchant is H_2O_2 : H_2O_2 : H_2O (5 : 1 : 1) at 26°C for 5 min.

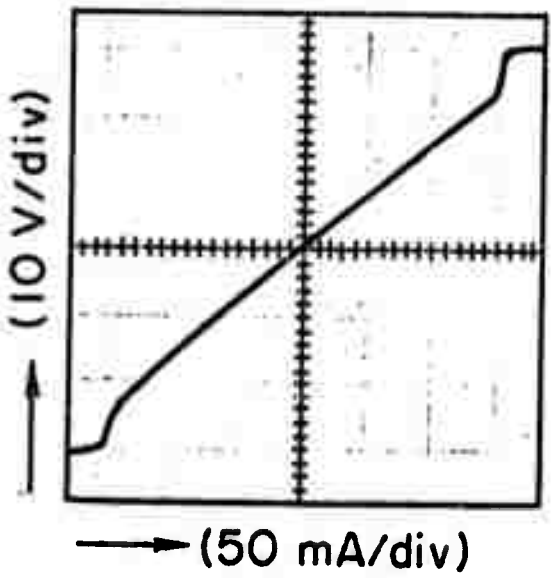

Figure III-1. I-V characteristic of the GaAs amplifier, taken between source and drain, with the input Schottky-barrier gate floating.

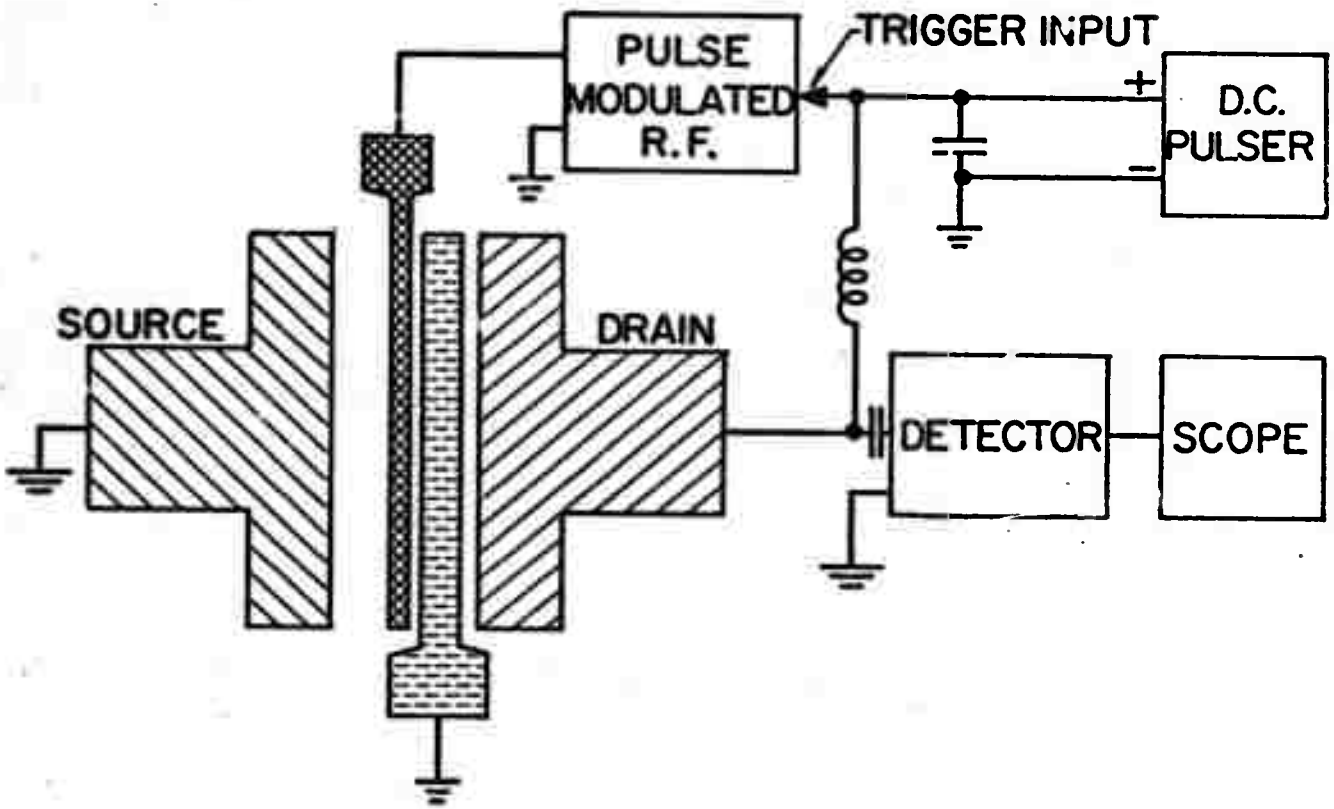

Figure III-2. RF testing circuit for the GaAs amplifier.

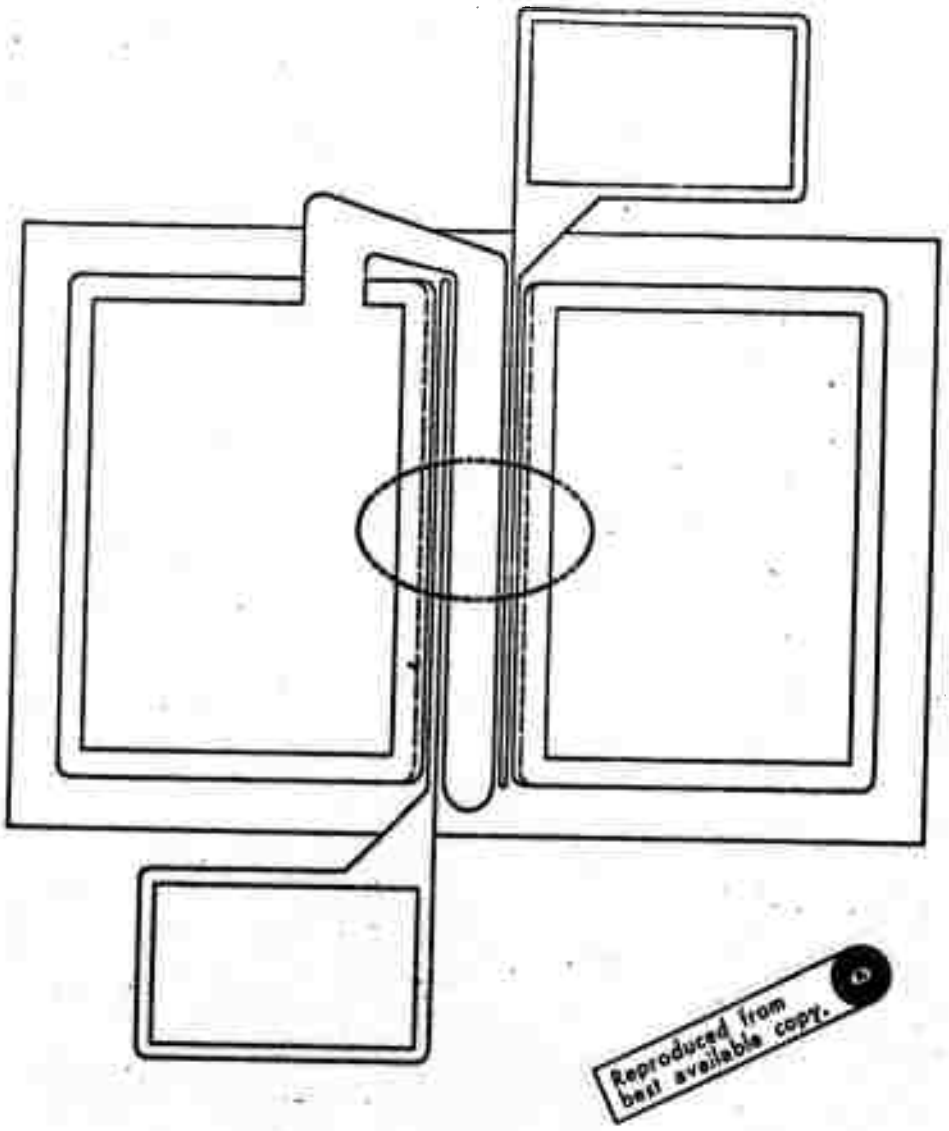

Reproduced from best available copy.

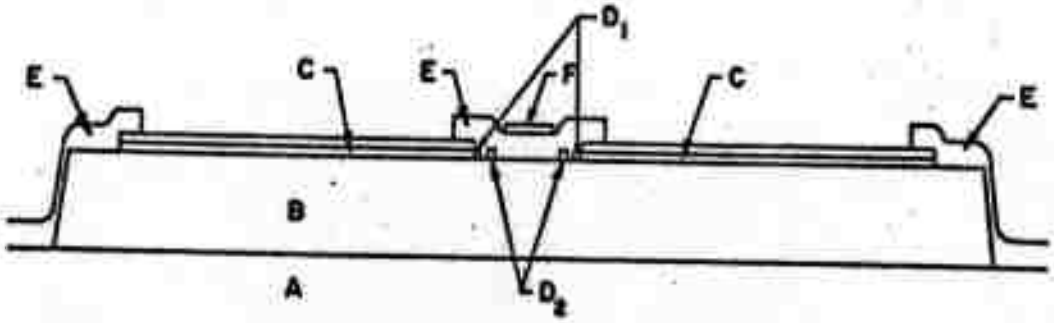

Figure III-3. Schematic view of the GaAs amplifier with Schottky-barrier input and output gates. A--semi-insulating GaAs substrate; B--n-type GaAs epitaxial layer; C--ohmic contacts; D_1--Schottky-barrier contact extension; D_2 Schottky-barrier gates; E--insulating layer; F--insulated gate.

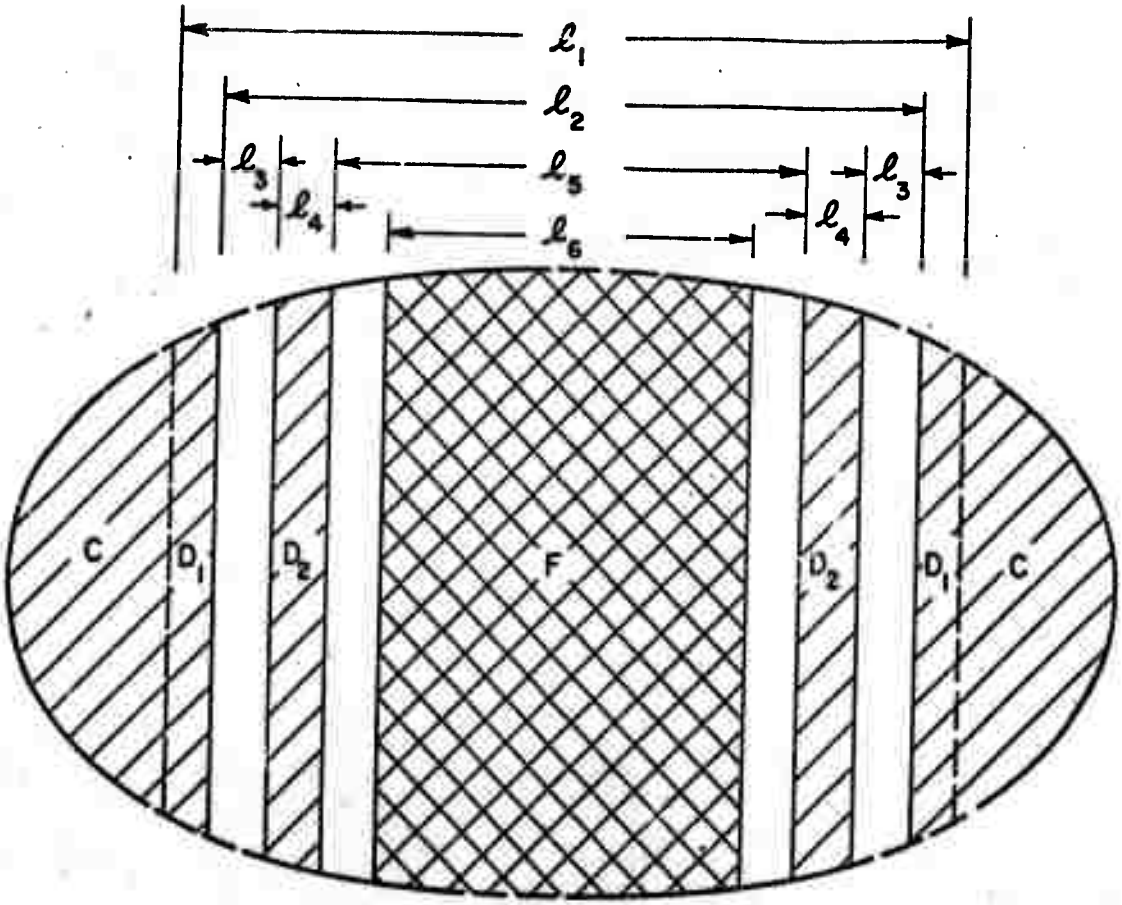

	I (μm)	II (μm)
ℓ_1	93	70
ℓ_2	85	65
ℓ_3	5	5
ℓ_4	5	5
ℓ_5	65	45
ℓ_6	56	36

Figure III-4. Blow-up of the center section of the amplifier.

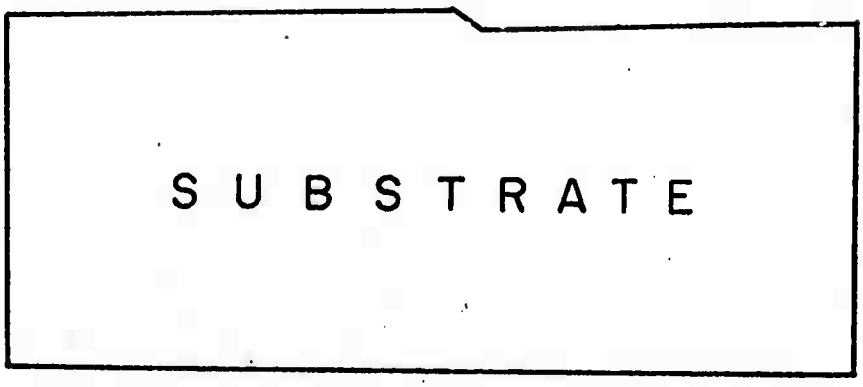

Figure III-5. Mesa profile on the <111>B face. Mesa step is 3.8 μm; etchant is H_2O_2 : H_2O_2 : H_2O (5 : 1 : 1) at 26°C for 5 min.

IV. RELATIONS BETWEEN DISLOCATIONS AND MECHANICAL PROPERTIES AND THE PRODUCTION AND CHARACTERIZATION OF DEFECT STRUCTURES IN COMPOUND SEMICONDUCTORS

R. H. Bube, W. D. Nix and A. L. Lin

A. PROGRAM OBJECTIVE

One of the objectives in this part of the research program is to devise techniques for modifying and characterizing the line defect structures in compound semiconductors, particularly GaAs, through high temperature mechanical deformation Our previous measurements of electrical conductivity, Hall and photo-Hall effect, photoconductivity and thermally stimulated conductivity indicate that the electrical properties are affected more by the heating necessary to achieve bending than by the bending itself, and that the properties are controlled primarily by the imperfections present in the crystal rather than by deformation-induced dislocations. We did find, however, that the photo-excited carrier lifetime and Hall mobility were appreciably changed by heating and bending. To interpret these data more fully, we have concentrated on an understanding of the photoconductivity characteristics of high-resistivity GaAs itself.

One of the major impressions received by surveying the literature and our own measurements on high-resistivity GaAs:Cr and GaAs:O is that a relatively large number of imperfection levels are common to almost all high-resistivity GaAs, regardless of the specific method of preparation, even if this method is labeled "no intentional impurities added." For example, five trapping states with depths between 0.2 and 0.4 eV have been identified and reported in "pure" high-resistivity GaAs, high-resistivity GaAs:Cr and GaAs:O. These trapping states, as well as a

number of others, appear to be independent of the specific method used to achieve high resistivity.

Although a number of investigations of the properties and associated energy levels of high-resistivity GaAs:Cr have been carried out, there is still some confusion about the location of the associated levels and the mechanism of the photoconductivity process. A number of investigations to date are summarized in Table I.

B. PROGRESS: HIGH RESISTIVITY GaAs:Cr

1. Materials

All samples of GaAs:Cr were grown by the sealed Czochralski technique and were purchased from Bell and Howell Co. Three as-grown samples (I24A, I36, and I41) were cut from different places in the same ingot. The heated sample (I24B) and the deformed sample (I25) described partially in previous reports were cut from the same place in the ingot as sample I24A. An additional as-grown sample (II2) was cut from a different ingot for comparison. Typical impurity contents in the ingots are summarized in Table II, as determined by mass spectrographic analysis. Although the material has been doped intentionally only with Cr, it may be noted that concentrations of C, O, Na, Al and S are of the same order of magnitude.

Table III shows a summary of the measurements made on each as-grown sample of GaAs:Cr.

2. Photocurrent Oscillations

The upper insert in Fig. 1 shows the I-V characteristics of sample I24A at 295°K in the dark and at 82°K under intrinsic photoexcitation. The boundaries of the cross-hatched region represent the maximum and

minimum values of the oscillating photocurrent observed at 82°K. The oscillation occurs in a range where the photocurrent has saturated with applied field, as is common in such phenomena. For an electric field of 47 V/cm, oscillations occur for photoexcitation with wavelength either $0.83\mu < \lambda < 1.06\mu$, or $1.39\mu < \lambda < 1.48\mu$, i.e., near the two maxima in the photoconductivity spectral response, corresponding to intrinsic and extrinsic excitation respectively. The curves of Fig. 1 show the variation of oscillation frequency and amplitude with applied field and light intensity. Such phenomena seem to result from a field-dependent trapping effect, but no direct evidence to this effect is yet available because of a lack of detailed knowledge about the imperfection levels present.

3. Dark Conductivity and Hall Effect

The activation energy for the variation of dark conductivity with temperature for the four as-grown GaAs:Cr samples is 0.68 ± 0.01 eV. The Hall mobility is approximately independent of temperature in the range 280°-330°K, but decreases with decreasing temperature below 280°K. The required np product to account for this decrease in Hall mobility by a two-carrier effect is at least three orders of magnitude larger than the n_i^2 value for GaAs, thus indicating that a simple two-carrier effect cannot account for the low temperature decrease in Hall mobility. The location of the Fermi level for each sample at 300°K, calculated from the Hall coefficient, is given in Table IV.

4. Photoconductivity Spectral Response

The spectral response of photoconductivity and Hall mobility are given in Figs. 2a and 2b for measurements at 295°K, and in Figs. 3a and 3b for measurements at 82°K. Intrinsic photoexcitation produces a

maximum at 1.43 eV at 295°K and at 1.48 ± 0.03 eV at 82°K; extrinsic photoexcitation produces a maximum at 0.9 eV at 295°K and at 0.86 eV at 82°K. The photoconductivity minimum which occurs at 1.0 eV at 295°K is actually dominated by hole conductivity at 82°K. The missing data between 1.3 and 1.45 eV occur in a range in which the measured value depends on previous sample history with very long time constants.

5. Photoconductivity vs. Temperature

The temperature dependence of photoconductivity for intrinsic photoexcitation (at the photoconductivity maximum) and the associated photo-Hall mobility are given in Figs. 4a and 4b. Similar data for extrinsic photoexcitation (again at the photoconductivity maximum) are given in Figs. 5a and 5b. Apparent activation energies for the various samples and modes of photoexcitation are summarized in Table IV.

The temperature dependence of the photoconductivity and photo-Hall mobility for extrinsic excitation at 1.11 eV are shown in Figs. 6a and 6b. The temperature at which the photo-Hall mobility changes sign is also listed in Table IV.

6. Photoconductivity Models

It is evident from the above results that we are dealing with a multilevel (probably a minimum of 3 levels) system with a delicate balance between n- and p-type conductivity. The various samples measured indicate different stages along this balance and the detailed data should provide a guide to interpretation. The essential qualitative features of the model were described in the previous report and need not be repeated here.

The temperature dependence of photoconductivity shown in Figs. 4 and 5 has been reported in other investigations of various types of high-

resistivity GaAs crystals. For example, in measurements on "pure" high-resistivity GaAs, Bube and MacDonald[15] report three crystals for which the ln photoconductivity increases linearly with 1/T. Effective activation energies for photoconductivity lie between 0.077 and 0.100 eV; photo-Hall measurements show that the activation energies for electron density lie between 0.083 and 0.095 eV. Data on 8 other n-type high-resistivity crystals in the same report indicate photoconductivity activation energies between 0.072 and 0.105 eV. Omelianovski[16] has shown that the ln photoconductivity increases linearly with 1/T in GaAs:O with effective activation energy of 0.06 - 0.07 eV. Instances in high-resistivity GaAs crystals in which the ln photoconductivity decreases with 1/T (like those shown in Fig. 6) have been reported in p-type GaAs:Si:Cu crystals by Blanc et al.[17] The spread of effective activation energies is large but many values in the range of 0.08 - 0.11 eV are reported. The effective activation energy for several of the curves shown in Fig. 6 is of the order of 0.06 eV. A previous attempt to integrate these results suggests[15] that centers lie 0.09 eV above the valence band which act as sensitizing centers for n-type photoconductivity and recombination centers for p-type photoconductivity. The fact that this activation energy appears to be varying in a systematic way in our present samples of GaAs:Cr (as seen in Figs. 4, 5 and Table IV) sugges, however, that the location of a single discrete level is not responsible for this behavior.

We are in the process of exploring a number of fundamental photoconductivity models with 1 or more recombination levels dominating, and for intrinsic or extrinsic photoexcitation. A 1-level model in the large-signal Shockley-Read treatment provides a mechanism for a variation of ln photoconductivity increasing with 1/T; such a variation occurs for

n-type photoconductivity if the level lies below the dark Fermi level, and it occurs for p-type photoconductivity if the level lies above the dark Fermi level. In either case the activation energy corresponds to the positive difference between the energy of the recombination level and the energy of the Fermi level, and the photoconductivity is predicted to vary linearly with light intensity.

General expressions can be readily derived for the photoconductivity behavior of multilevel systems for intrinsic or extrinsic photoexcitation. The difficult step in the final solution of each problem is the derivation of the relationship between the photoexcited electron density and the photoexcited hole density. To apply the approach of calculating the change in occupancy of each level to account in a detailed way for the difference between Δn and Δp, as is done in the Shockley-Read model above, requires extensive calculations. Another method of establishing the relationship between Δn and Δp, which may be useful in certain cases, is to attempt to derive this relationship from simple charge neutrality considerations, assuming that two or more of the levels involved determine the location of the equilibrium Fermi level and that the relationship between dark electron and hole densities can be used also in photoexcitation for a relationship between Δn and Δp. When this approach is applied to a 2-level model with levels lying E_1 (below the Fermi level) and E_2 (above the Fermi level) below the conduction band, the ln photoconductivity is predicted to decrease linearly with 1/T with an activation energy of either $E_2/2$ or $(E_1-E_G+2E_2)/2$, whichever is the larger, and the photocurrent is predicted to vary as the square-root of the excitation intensity. Similar models will be explored further.

C. PROGRESS: HIGH RESISTIVITY GaAs:O

Characterizing measurements were made on a crystal of high-resistivity GaAs:O for three reasons: (1) to see what characteristic differences, if any, existed between high-resistivity GaAs:Cr and GaAs:O; (2) because preliminary investigation of photoconductivity in GaAs:O crystals had already been carried out by Omelianovski; and (3) because a concurrent investigation of defect states in GaAs:O by electrotransmission methods is being underteken here by Jonath.[18]

1. Materials

The crystals of GaAs:O used were grown by the Monsanto Co., St. Louis.[19] Attempts were made to very the incorporated oxygen impurity concentration by varying the oxygen pressure in the reactor tube during the crystal growth; mass spectrographic analysis of the crystals used, however, indicates only about 5 ppm of incorporated oxygen impurity.

2. Photocurrent Oscillations

At 82°K under intrinsic photoexcitation, the I-V characteristic is ohmic up to about 90 V/cm and oscillations are observed at about 120 V/cm.

3. Dark Conductivity and Hall Effect

The activation energy measured from the temperature dependence of dark conductivity is 0.47 eV between 295° and 330°K. As in the GaAs:Cr sample, the Hall mobility is constant over this temperature range and then decreases with decreasing temperature below this range. The Fermi level location calculated from the Hall coefficient at 300°K is 0.58 eV.

4. Photoconductivity Spectral Response

Figure 7 shows the spectral response curves for photoconductivity and photo-Hall mobility measured at 295° and 213°K. The curve at 213°K differs only slightly from that at 295°K.

The spectral response curve measured at 82°K is quite different. Figure 8a and 8b shows the spectral response for photoconductivity and photo-Hall mobility as measured 3 min and 15 min after photoexcitation (very long time constants over part of spectral range) in two different ways: (1) measuring from high to low photon energy on a previously heated and cooled (in the dark) crystal, and (2) measuring from low to high photon energy on a previously heated and cooled (in the dark) crystal. The results can be interpreted to indicate two states for the crystal: a higher sensitivity n-type state (except for the range between 1.1 and 1.2 eV) which is encountered at high energies when measuring from high-to-low photon energies, and is encountered at low energies when measuring from low-to-high photon energies, i.e., over that portion of the spectral range encountered before exposing the sample to wavelengths in the 1.0-1.3 eV range; and a lower sensitivity p-type state to which the higher sensitivity n-type state is reduced by exposure to 1.0-1.3 eV photons. The photoconductivity in the p-type state is about two orders of magnitude smaller than that in the n-type state. Comparison of the low-temperature spectral response for GaAs:O with that for GaAs:Cr in Fig. 3 indicates qualitative similarity with some quantitative differences.

5. Photoconductivity vs. Temperature

Figures 9a and 9b show the temperature dependence of photoconductivity and photo-Hall mobility for intrinsic excitation. The upper curve

represents the crystal in its high-sensitivity state. The behavior is very similar to the curves of Fig. 4 for the GaAs:Cr crystal, and the effective activation energy is 0.066 eV. The lower curve represents the temperature variation of photoconductivity in a low-sensitivity state induced by exposure to 1.08 eV radiation for 1 hr at 82°K. This quenching process, as described below, is very long lived at low temperatures, and the low-sensitivity quenched state persists long after the removal of the quenching radiation. Upon heating, however, Fig. 9a shows a rapid and dramatic recovery from the low-sensitivity quenched state to the high-sensitivity state when the temperature exceeds 105°K which is completed by 122°K. Reference to the thermally stimulated current curves in Fig. V-7 of our previous report shows that this is the temperature range in which the first major trap emptying occurs in GaAs:Cr; data for GaAs:O indicate quite similar behavior. We may conclude that the low-temperature low-sensitivity quenched state which persists is due to a large density of photoexcited holes transferred to fast-recombination centers by the quenching radiation, corresponding to electrons trapped in the electron traps.

6. Optical Quenching of Photoconductivity

Figure 10 shows optical quenching spectra for GaAs:O at 80° and 213°K, i.e., below and above the critical temperature for the above long-lived effect. The 213°K spectrum is quite similar to that measured for GaAs:Cr (see Fig. V-6 in our previous report), with the possible shift by 0.1 eV to higher energies for the GaAs:O.

At 80°K optical quenching in GaAs:O is quite different from that in GaAs:Cr. The onset of optical quenching is at 0.5 eV with an abrupt

increase at about 0.77 eV. In the spectral range from 0.5 to 1.13 eV, the quenching light produces only quenching of the photocurrent without any attendant stimulation; both the quenching and recovery processes are relatively fast. When the quenching photon energy exceeds 1.13 eV, however, three processes are found: (1) a fast stimulation, (2) a fast quenching, and (3) a slow and very large quenching, corresponding to the effects described above. At 1.18 eV, for example, the fast quenching produces 7.5 percent quenching; after 1 hr of exposure, the slow quenching has produced 98 percent quenching with a decrease in the Hall mobility from 1.5×10^4 to 1.8×10^2 $cm^2/V\text{-}sec$. If the quenching light is turned off after this exposure, leaving the intrinsic primary photoexcitation on, the Hall mobility increases to 8×10^2 $cm^2/V\text{-}sec$ and the photoconductivity increases from 1.9×10^{-6} to 2.8×10^{-6} $(ohm\text{-}cm)^{-1}$. Even after a recovery period of 4-1/2 hrs at 80°K, the photoconductivity is only 6.8×10^{-6} $(ohm\text{-}cm)^{-1}$ and the Hall mobility is only 1.4×10^3 $cm^2/V\text{-}sec$.

D. FUTURE WORK: HIGH RESISTIVITY GaAs:Cr

(1) Continued development of a suitable model and interpretation of the data in terms of that model.

(2) Comparison of details of heat-treated and deformed samples of GaAs:Cr with data on as-grown crystals with similar lifetime characteristic, i.e., do heat-treatment and deformation essentially do the same thing as happens in a varisble way in samples taken from different portions of an as-grown ingot?

(3) Determination of the cause of differences between GaAs:Cr and GaAs:O.

REFERENCES

1. G. R. Cronin and R. W. Haisty, J. Electrochem. Soc. 111, 874 (1964).
2. W. J. Turner and G. D. Petit, Bull. Am. Phys. Soc. 9, 269 (1964).
3. C. E. Jones and A. R. Hilton, J. Electrochem. Soc. 113, 504 (1966).
4. E. W. Williams and D. M. Blacknall, Trans. Metall. Soc. AIME 239, 387 (1967).
5. R. F. Broom, J. Appl. Phys. 38, 3483 (1967).
6. D. R. Heath, P. R. Selway and C. C. Tooke, Brit. J. Appl. Phys. 1, 29 (1968).
7. G. A. Allen, Brit. J. Appl. Phys. 1, 593 (1968).
8. T. Inone and M. Ohyama, Jap. J. Appl. Phys. 8, 1362 (1969).
9. N. M. Kolchanova, D. N. Nasledov, M. A. Mirdkhalilova and V. Yu. Ibrugimov, Sov.Phys.-Semicond. 4, 294 (1970).
10. J. G. Harper, H. E. Matthews and R. H. Bube, J. Appl. Phys. 41, 3182 (1970).
11. O. V. Tretyak, Sov. Phys.-Semicond. 4, 517 (1970).
12. V. M. Gontar', G. A. Egiazaryan, V. S. Rubin, V. I. Murygin and V. I. Stafeev, Sov. Phys.-Semicond. 5, 939 (1971).
13. S. S. Li and C. I. Huang, J. Appl. Phys. 43, 1757 (1972).
14. G. P. Peka and Karkhanin, Sov. Phys.-Semicond. 6, 261 (1972).
15. R. H. Bube and H.E. MacDonald, Phys. Rev. 128, 2062 (1962).
16. E. Omelianovski, unpublished results.
17. J. Blanc, R. H. Bube and H. E. MacDonald, J. Appl. Phys. 32, 1666 (1961).
18. A. D. Jonath, unpublished results.
19. Supplied through the kindness of Warren O. Groves.

TABLE I

Summary of Investigations of Deep Levels in High Resistivity GaAs:Cr

Year	Authors	Ref. No.	Type[a]	Hall Mobility, $cm^2/V\text{-}sec$, 300°K	Activation Energy, eV E	Method Used
1964	Cronin and Haisty	1	n_H, p_T	600-2000	0.79	Dark conductivity vs. T
	Turner and Petit	2			0.8 (77°K)	Photoluminescence
1966	Jones and Hilton	3			0.72 (80°K)	Photoabsorption
1967	Williams and Blacknall	4			0.85 (20°K)	Photoluminescence
	Broom	5	n_H	1000	0.89 (290°K)	Photoconductivity spectrum maximum
					0.86 (80°K)	Photoconductivity spectrum maximum
1968	Heath, Selway and Tooke	6			0.87 (300°K)	Photoconductivity spectrum maximum
	Allen	7	n_H	1000-3000	0.81±0.02 $-8x10^{-4}T$ (T 100°K)	Photoconductivity threshold
					0.8	Dark conductivity vs. T
					0.79(77°K)	Photoluminescence
					0.8 (77°K)	Cathodoluminescence
					0.89(77°K)	Photoconductivity spectrum maximum
1969	Inone and Ohyama	8	n_H	1000	0.86, 1.18 (195°K)	Photoconductivity spectrum maxima
1970	Kolchanova et al	9	n_H		0.85 (300°K)	Photoconductivity spectrum maximum
	Harper, Matthews and Bube	10	n_H, p_T		0.56, 0.9, 1.2 (293°K)	Photothermoelectric effect
	Tretyak	11	n_H	600-1000	0.86 (300°K)	Photoconductivity spectrum maximum
					0.97 (83°K)	Optical Quenching of Photoconductivity
1971	Gontar' et al.	12	n_H		0.7-0.8	Dark conductivity vs. T
					0.85 (293°K)	Photoconductivity spectrum maximum
					0.89 (145°K)	Photoconductivity spectrum maximum
1972	Li and Huang	13	n_H	150-450	Single acceptor near gap middle	Photomagnetoelectric effect
	Peka and Karkhanin	14	n_H		0.8 (77°K)	Photoluminescence
					Shifts with different donors	

TABLE II

Summary of Mass Spectrometric Analyses of Impurities Present in Cr-Doped Sealed System GaAs

Element	Typical Detection Limit ppma	Average Concentration ppma
Li	0.01	$<$ 0.1
B	0.05	$<$ 0.1
C	0.05	1.3
N	0.05*	$<$ 0.1
O	0.05*	2.4
F	0.05	$<$ 0.1
Na	0.5	2.0
Al	0.1	1-5
Si	0.05	0.5
P	0.05	$<$ 0.2
S	0.1	1.4
Cl	0.1	$<$ 0.1
K	0.1	$<$ 0.5
Ca	0.05	$<$ 0.1
Cr	0.1	3.5
Fe	0.1	$<$ 0.5
Ni	0.1	$<$ 0.5
Cu	0.05	$<$ 0.1
Zn	0.1	$<$ 0.1

Note: All other elements were not detected with detection limits of approximately 0.2 ppma.

* Plate sensitivity; does not take into account outgassing of instrument, oxidized surfaces, etc.

TABLE III

Summary of Our Measurements on GaAs:Cr Crystals

Sample No.	Dark Con. vs. T	Photoconductivity Spectrum 295°K	Photoconductivity Spectrum 82°K	Photoconductivity vs. T Intrinsic	Photoconductivity vs. T Extrinsic	Photoconductivity vs. T 1.11 eV	Photocon. vs. Light Intensity	Optical Quenching 295°K	Optical Quenching 82°K	TSC	Oscill. in Photocur
I24A[a]	X	X	X	X	X	X	X	X	X	X	X
I24B[b]	X	X	X	X	X	X	X	X	X	X	
I25[c]	X	X	X	X	X	X	X	X	X	X	
I36[a]	X	X	X	X	X	X	X				
I41[a]	X	X	X	X	X	X	X				
II2[a]	X	X	X	X	X	X	X				

[a] As grown

[b] Heated but not deformed

[c] Deformed

TABLE IV

Summary of Data on GaAs:Cr As-Grown Crystals

Sample No.	295°K Dark Con., $(ohm\text{-}cm)^{-1}$	295°K Dark Hall Mobility, $cm^2/V\text{-}sec$	295°K Dark Fermi Level, eV	Effective Activation Energy for Photocon. vs. T, eV: Intrinsic	Effective Activation Energy for Photocon. vs. T, eV: Extrinsic	Temperature at which Hall Mobility changes sign for 1.11 eV photon excitation, °K
I24A	5.6×10^{-9}	1700	0.605	0.051	0.067	114
I36	3.4×10^{-9}	1950	0.615	0.04	0.055	120
I41	3.6×10^{-9}	2320	0.621	0.028	0.054	127
II2	1.4×10^{-9}	1700	0.638	0.018	0.00	119

FIGURE CAPTIONS

Figure IV-1. Variation of oscillation frequency and amplitude with excitation intensity and applied electric field for I24A at 82°K. The insert shows the I-V characteristic in the dark at 295°K (lower curve) and under intrinsic photoexcitation at 82°K. The cross-hatched region represents the region of oscillations.

Figure IV-2a. Photoconductivity spectral response curves at 295°K.

Figure IV-2b. Variation of Hall mobility with exciting photon energy at 295°K, corresponding to the photoconductivity curves of Fig. 2a.

Figure IV-3a. Photoconductivity spectral response curves at 82°K.

Figure IV-3b. Variation of Hall mobility with exciting photon energy at 82°K, corresponding to the photoconductivity curves of Fig. 3a.

Figure IV-4a. Temperature dependence of dark conductivity and intrinsic photoconductivity.

Figure IV-4b. Temperature dependence of Hall mobility under intrinsic photoexcitation, corresponding to the photoconductivity curves of Fig. 4a.

Figure IV-5a. Temperature dependence of dark conductivity and extrinsic photoconductivity, corresponding to extrinsic maximum.

Figure IV-5b. Temperature dependence of Hall mobility under extrinsic photoexcitation corresponding to extrinsic maximum, for the photoconductivity curves of Fig. 5a.

Figure IV-6a. Temperature dependence of dark conductivity and extrinsic photoconductivity, corresponding to excitation by 1.11 eV photons.

Figure IV-6b. Temperature dependence of Hall mobility under extrinsic photoexcitation corresponding to 1.11 eV photons, for the photoconductivity curves of Fig. 6a.

Figure IV-7. Photoconductivity spectral response and variation of photo-Hall mobility with photon energy at 295° and 213°K for GaAs:O crystal.

Figure IV-8a. Photoconductivity spectral response curves at 82°K for GaAs:O crystal: measured from high to low photon energies, reading after 3 min (o), and after 15 min (Δ); measured from low to high photon energies, reading after 3 min (•), and after 15 min (▲).

Figure IV-8b. Photo-Hall mobility vs. photon energy for GaAs:O crystal at 82°K: measured from high to low photon energies, reading after 3 min (o), and after 15 min (Δ); measured from low to high photon energies, reading after 3 min (•), and after 15 min (▲).

Figure IV-9a. Temperature dependence of photoconductivity for GaAs:O crystal, for intrinsic photoexcitation (Δ); and for intrinsic photoexcitation after quenching with 1.08 eV photons for 1 hr (o) at 82°K, measured while warming.

Figure IV-9b. Temperature dependence of photo-Hall mobility in GaAs:O crystal, for intrinsic photoexcitation (Δ); and for intrinsic photoexcitation after quenching with 1.08 eV photons for 1 hr at 82°K, measured while warming, corresponding to curves of Fig. 9a.

Figure IV-10. Optical quenching spectra for GaAs:O crystal at 213°K and at 80°K. The data at 213°K are for two different relative quenching intensities of 1 (Δ) and 0.4 (o).

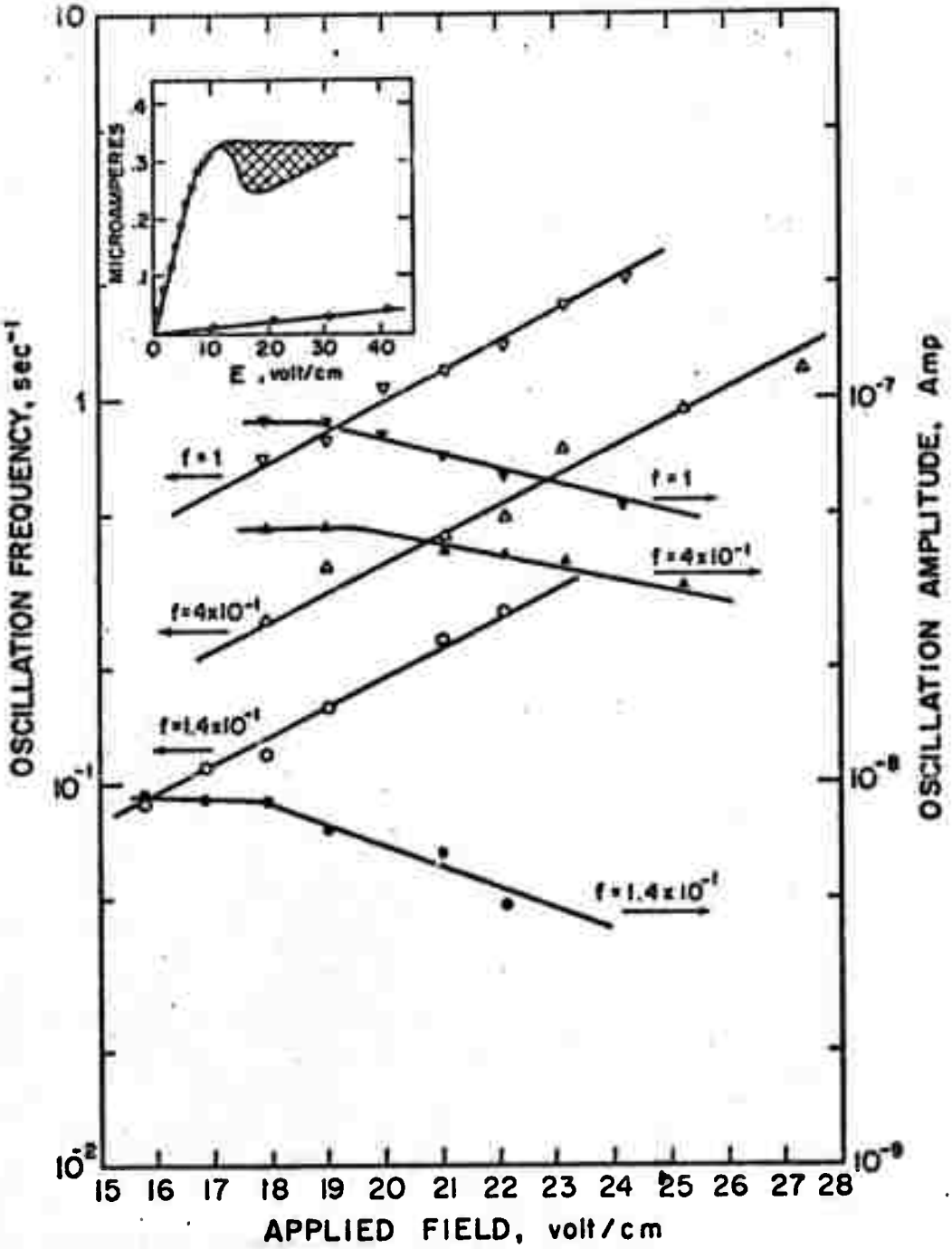

Figure 1. Variation of oscillation frequency and amplitude with excitation intensity and applied electric field for I24A at 82°K. The insert shows the I-V characteristic in the dark at 295°K (lower curve) and under intrinsic photoexcitation at 82°K. The cross-hatched region represents the region of oscillations. f = 1 corresponds to 1.7×10^{14} photons cm^{-2} sec^{-1}.

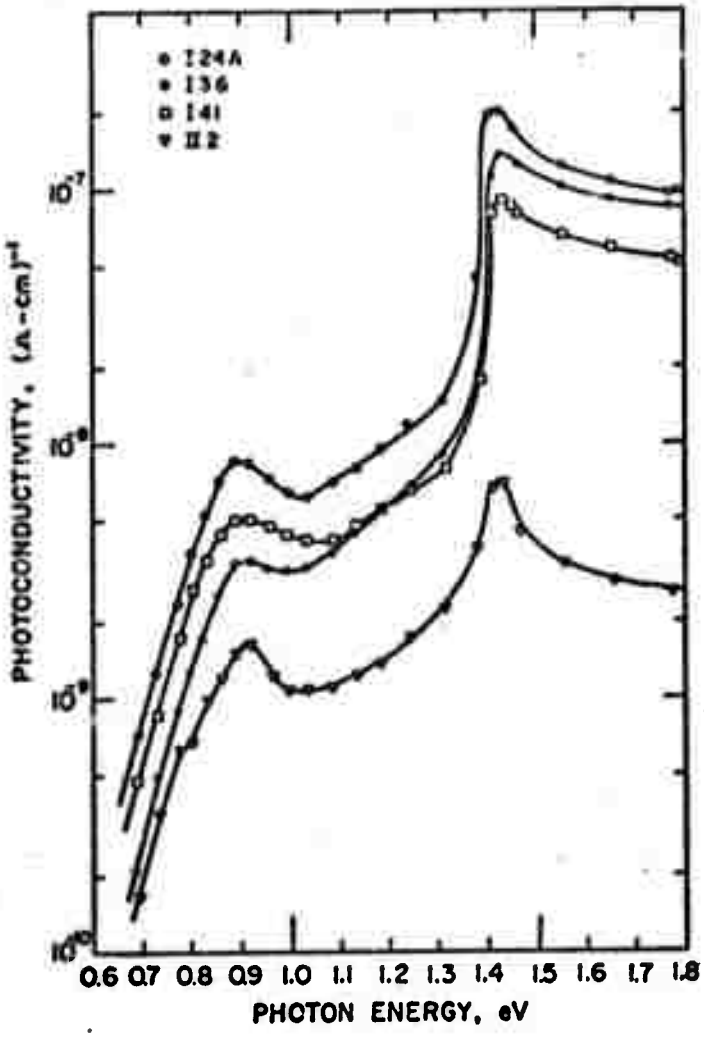

Figure 2a. Photoconductivity spectral response curves at 295°K.

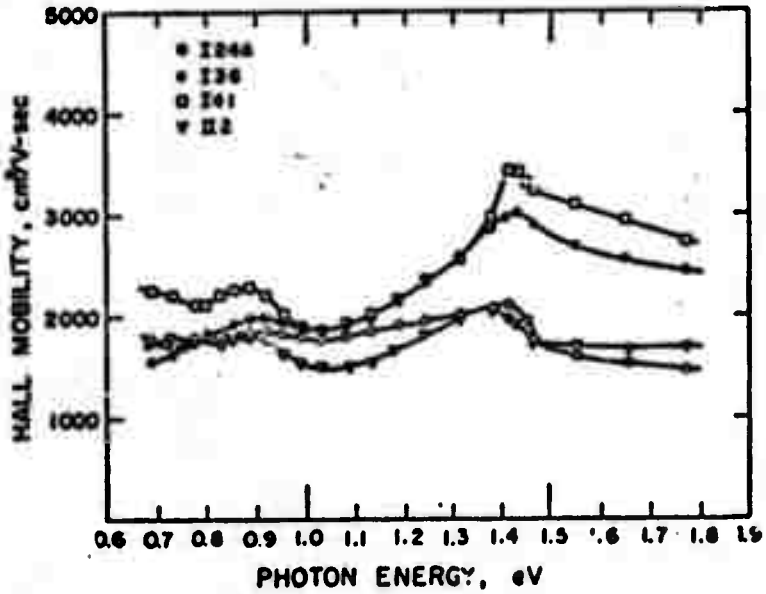

Figure 2b. Variation of Hall mobility with exciting photon energy at 295°K, corresponding to the photoconductivity curves of Figure 2a.

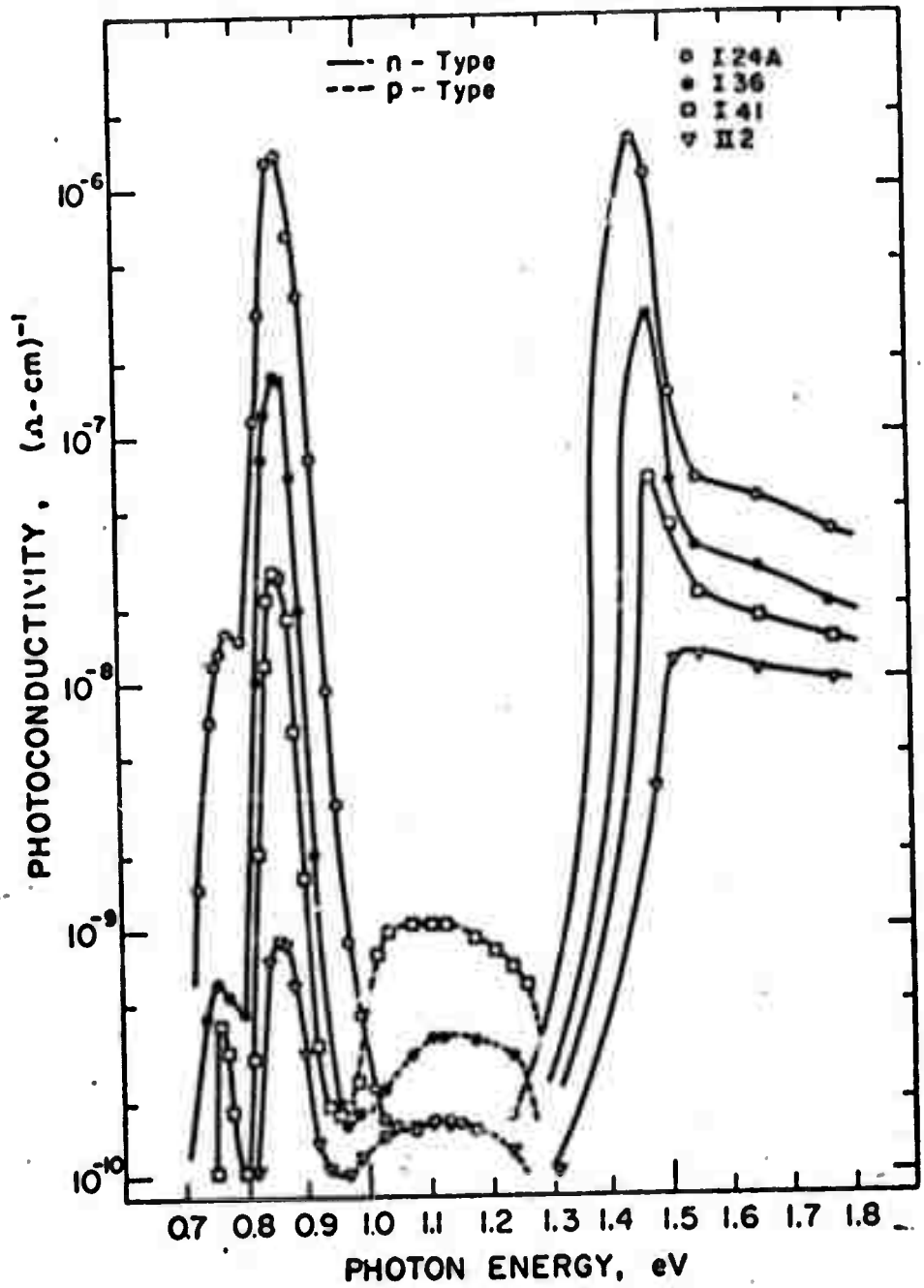

Figure 3a. Photoconductivity spectral response curves at 82°K.

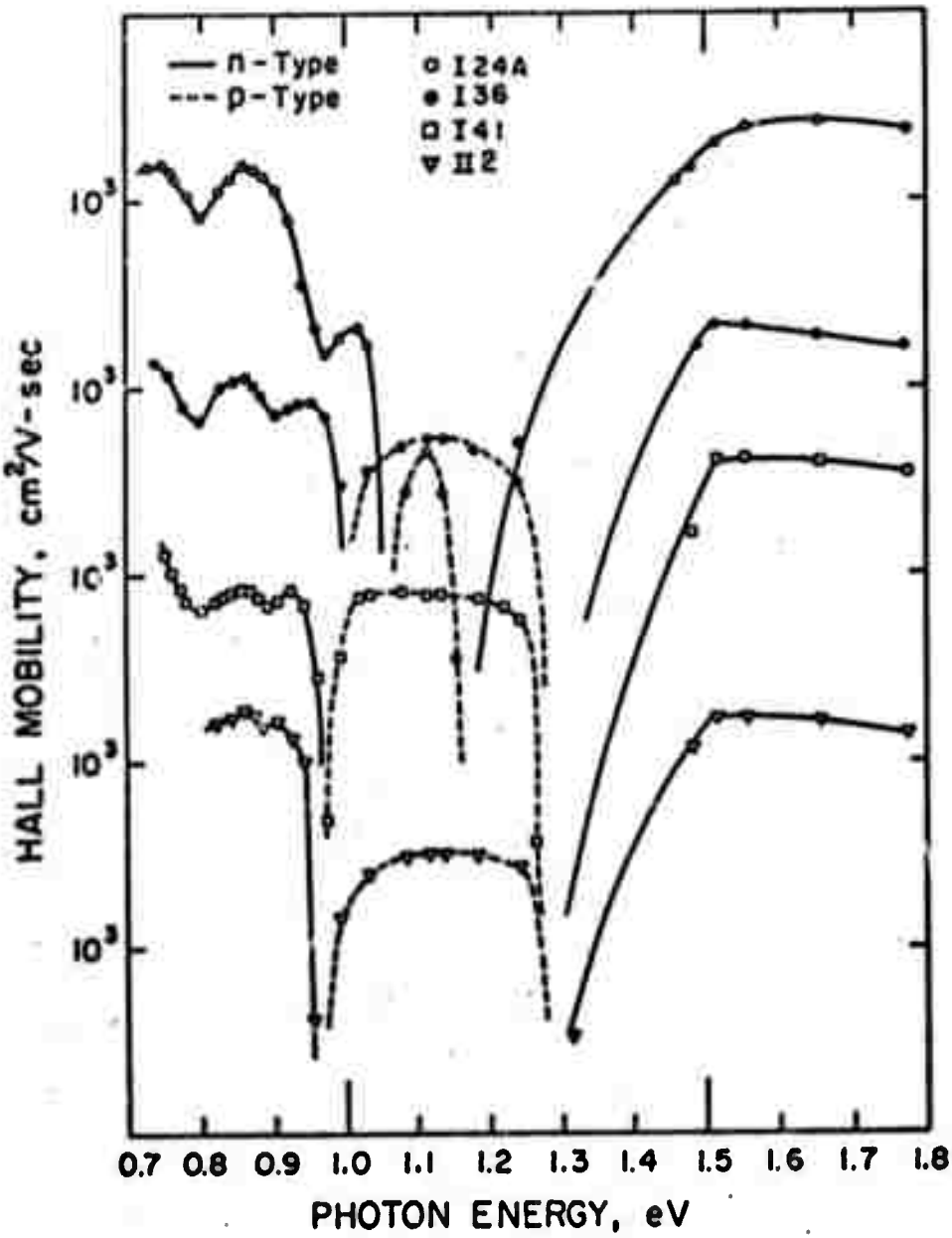

Figure 3b. Variation of Hall mobility with exciting photon energy at 82°K, corresponding to the photoconductivity curves of Figure 3a.

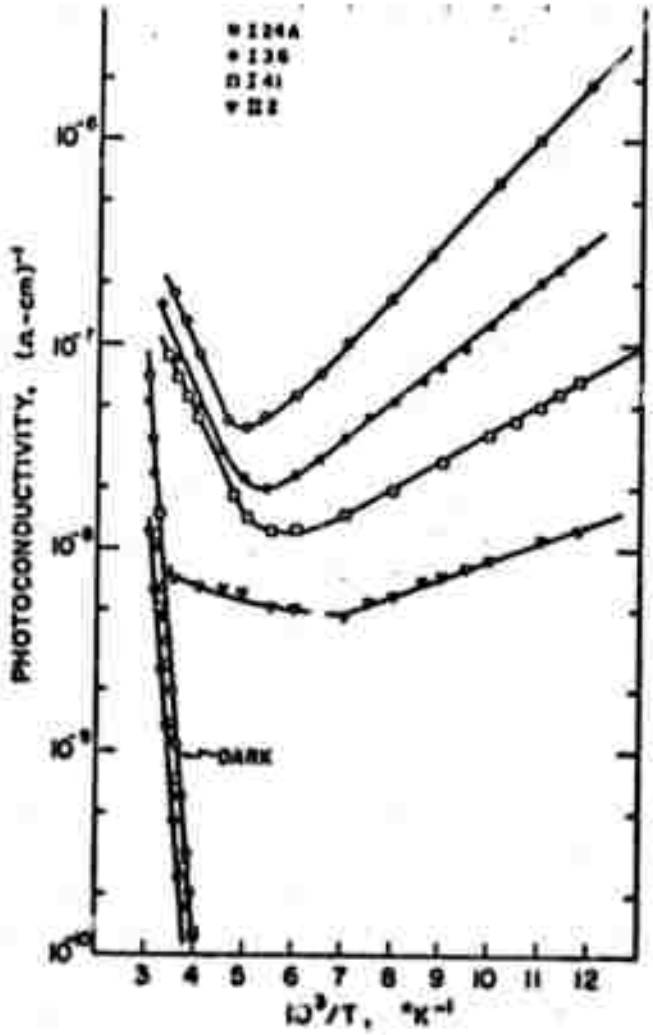

Figure 4a. Temperature dependence of dark conductivity and intrinsic photoconductivity.

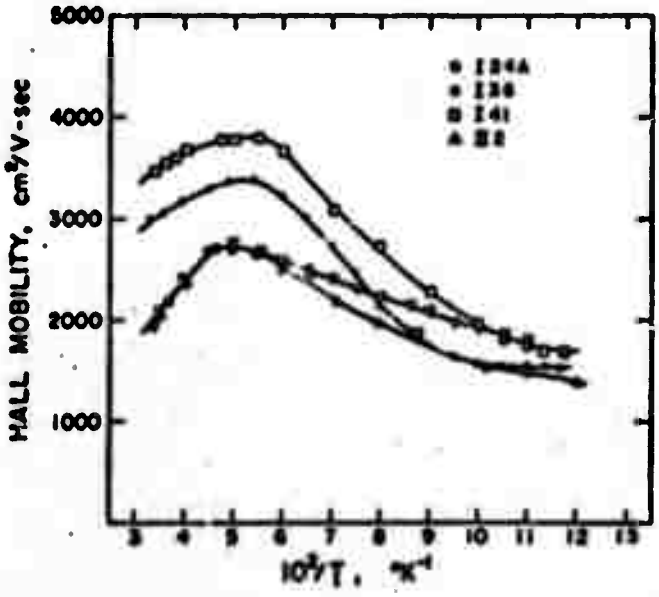

Figure 4b. Temperature dependence of Hall mobility under intrinsic photo-excitation, corresponding to the photoconductivity curves of Figure 4a.

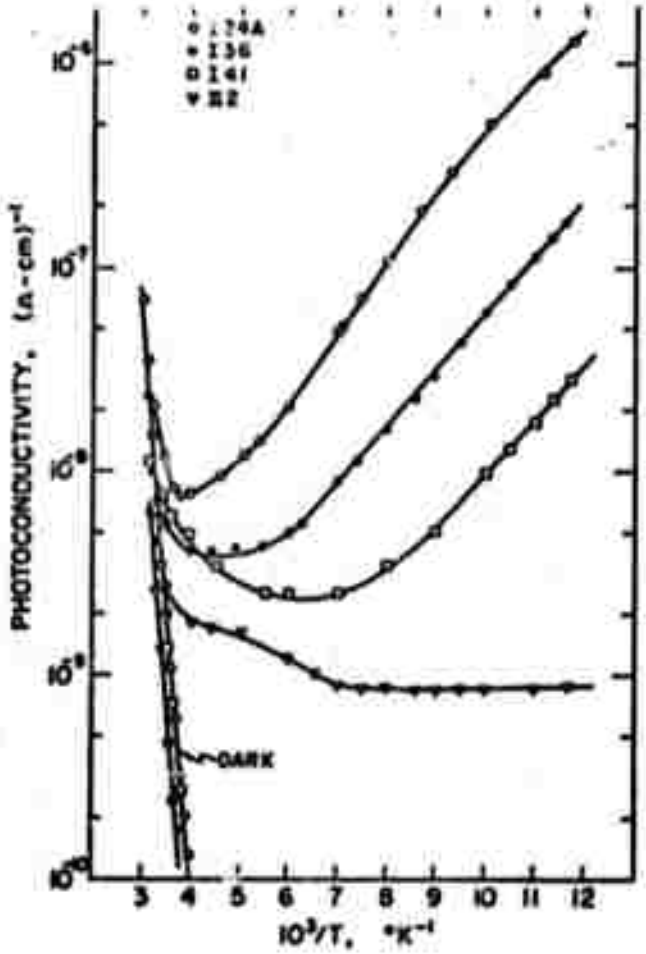

Figure 5a. Temperature dependence of dark conductivity and extrinsic photoconductivity, corresponding to extrinsic maximum.

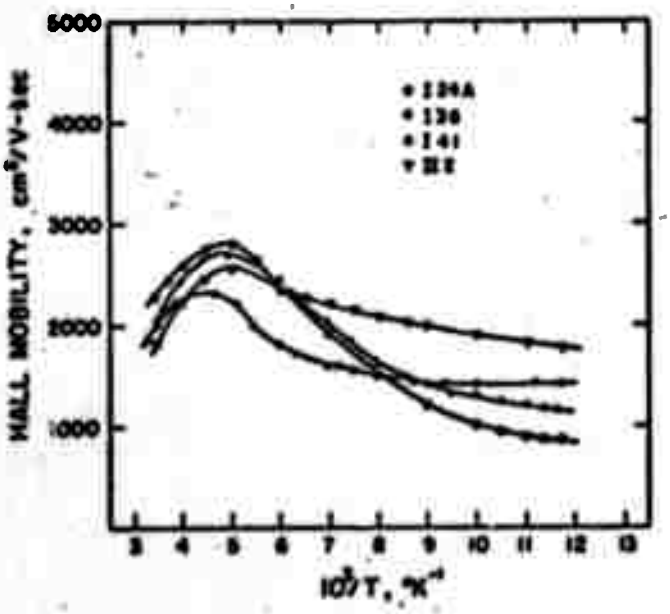

Figure 5b. Temperature dependence of Hall mobility under extrinsic photoexcitation corresponding to extrinsic maximum, for the photoconductivity curves of Figure 5a.

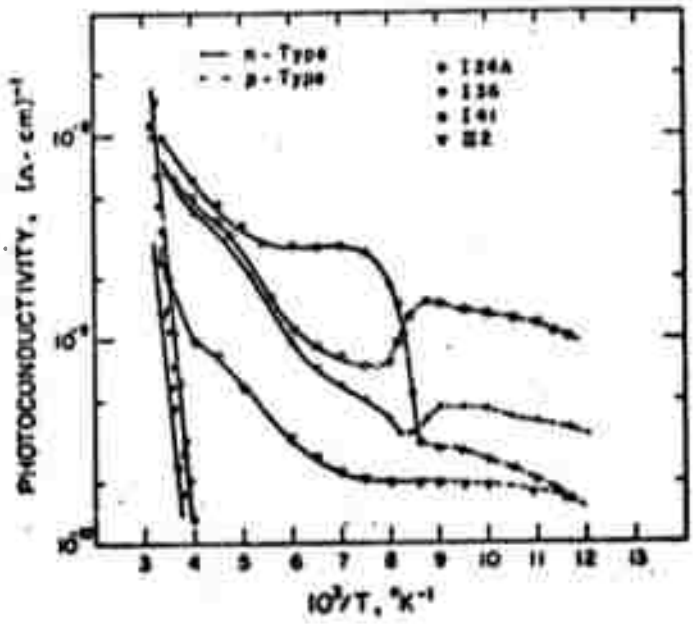

Figure 6a. Temperature dependence of dark conductivity and extrinsic photoconductivity, corresponding to excitation by 1.11 eV photons.

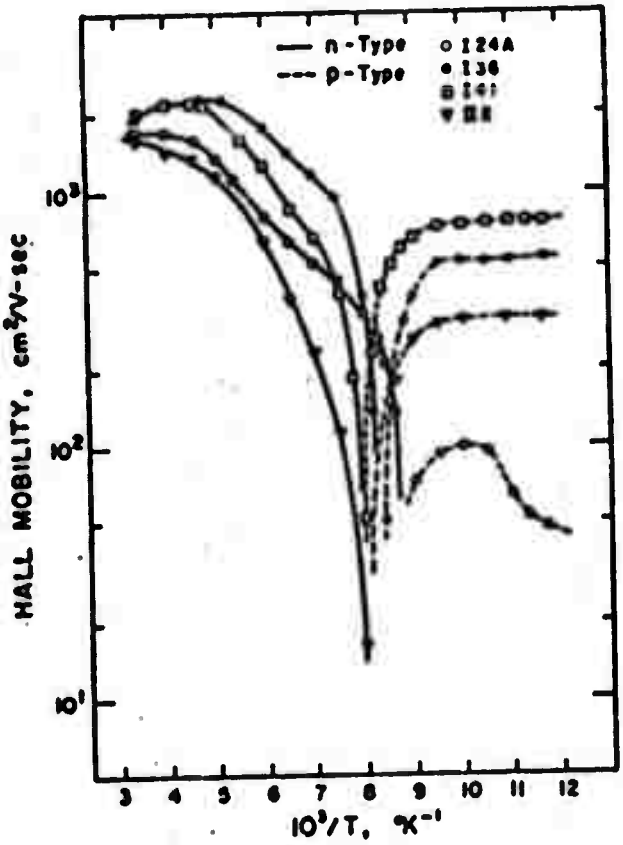

Figure 6b. Temperature dependence of Hall mobility under extrinsic photoexcitation corresponding to 1.11 eV photons, for the photoconductivity curves of Figure 6a.

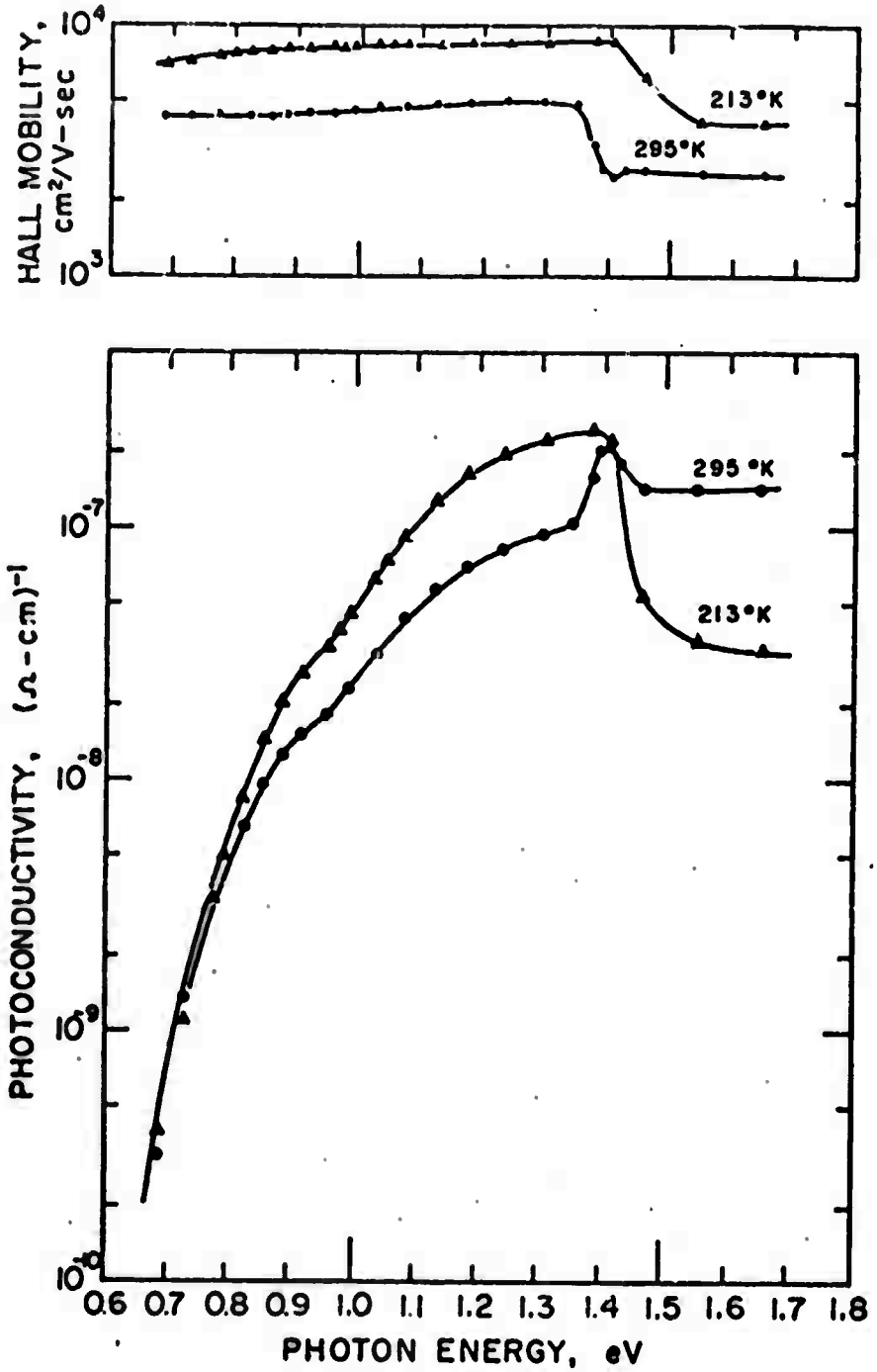

Figure 7. Photoconductivity spectral response and variation of photo-Hall mobility with photon energy at 295° and 213°K for GaAs:O crystal.

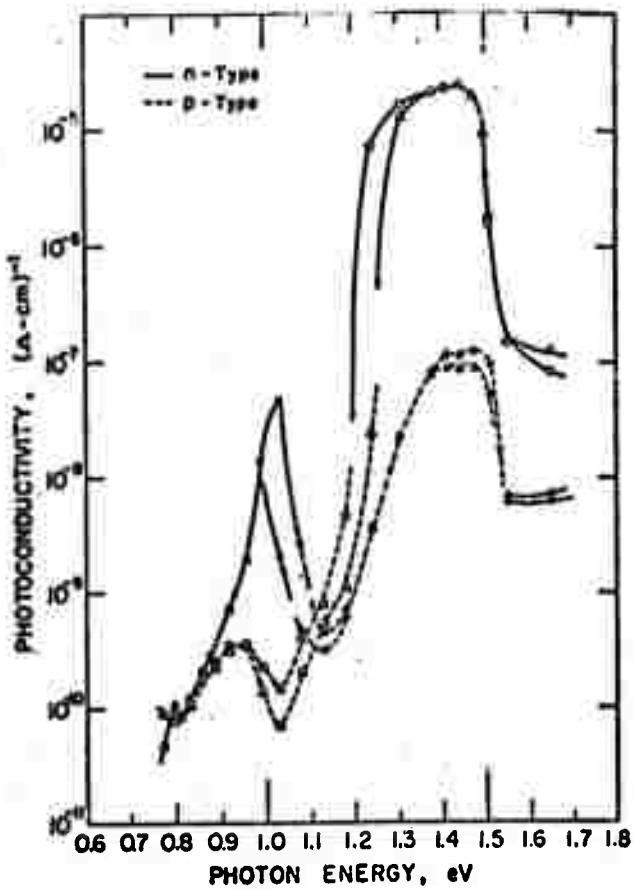

Figure 8a. Photoconductivity spectral response curves at 82°K for GaAs:O crystal: measured from high to low photon energies, reading after 3 min (o), and after 15 min (▲); measured from low to high photon energies, reading after 3 min (●), and after 15 min (▲).

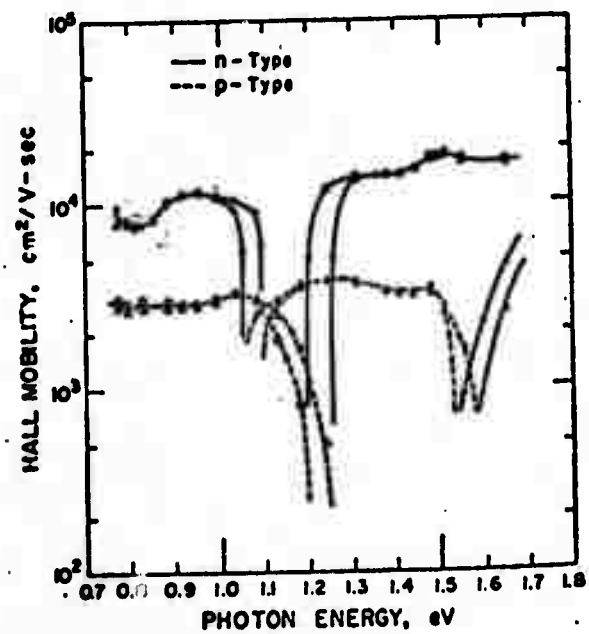

Figure 8b. Photo-Hall mobility vs. photon energy for GaAs:O crystal at 82°K: measured from high to low photon energies, reading after 3 min (o), and after 15 min (▲); measured from low to high photon energies, reading after 3 min (●), and after 15 min (▲).

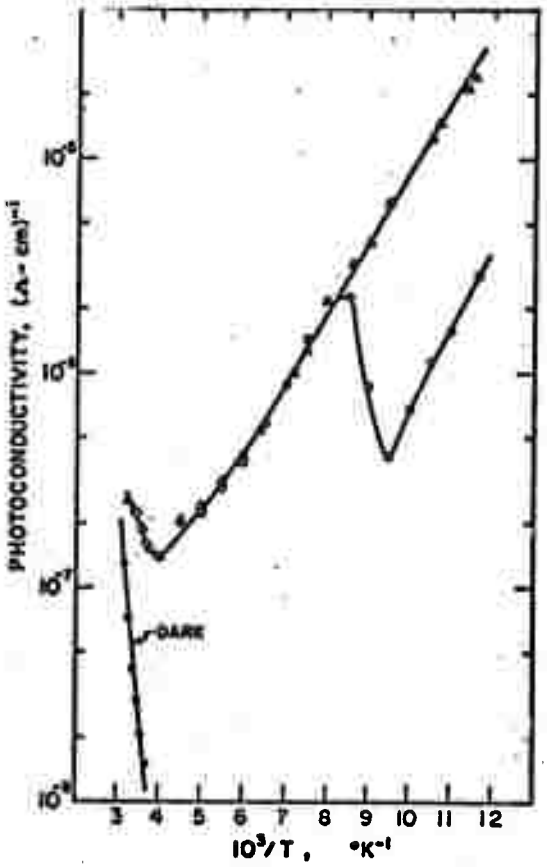

Figure 9a. Temperature dependence of photoconductivity for GaAs:O crystal, for intrinsic photoexcitation (▲); and for intrinsic photoexcitation after quenching with 1.08 eV photons for 1 hr (o) at 82°K, measured while warming.

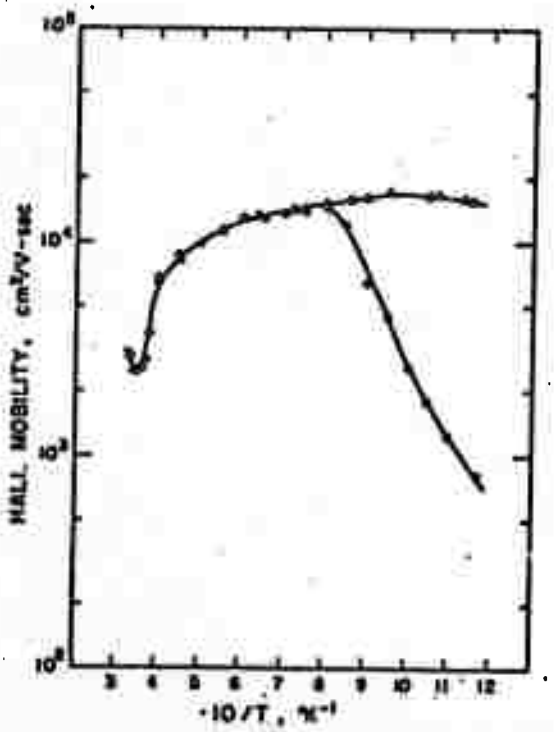

Figure 9b. Temperature dependence of photo-Hall mobility in GaAs:O crystal, for intrinsic photoexcitation (▲); and for intrinsic photoexcitation after quenching with 1.08 eV photons for 1 hr at 82°K, measured while warming, corresponding to curves of Figure 9a.

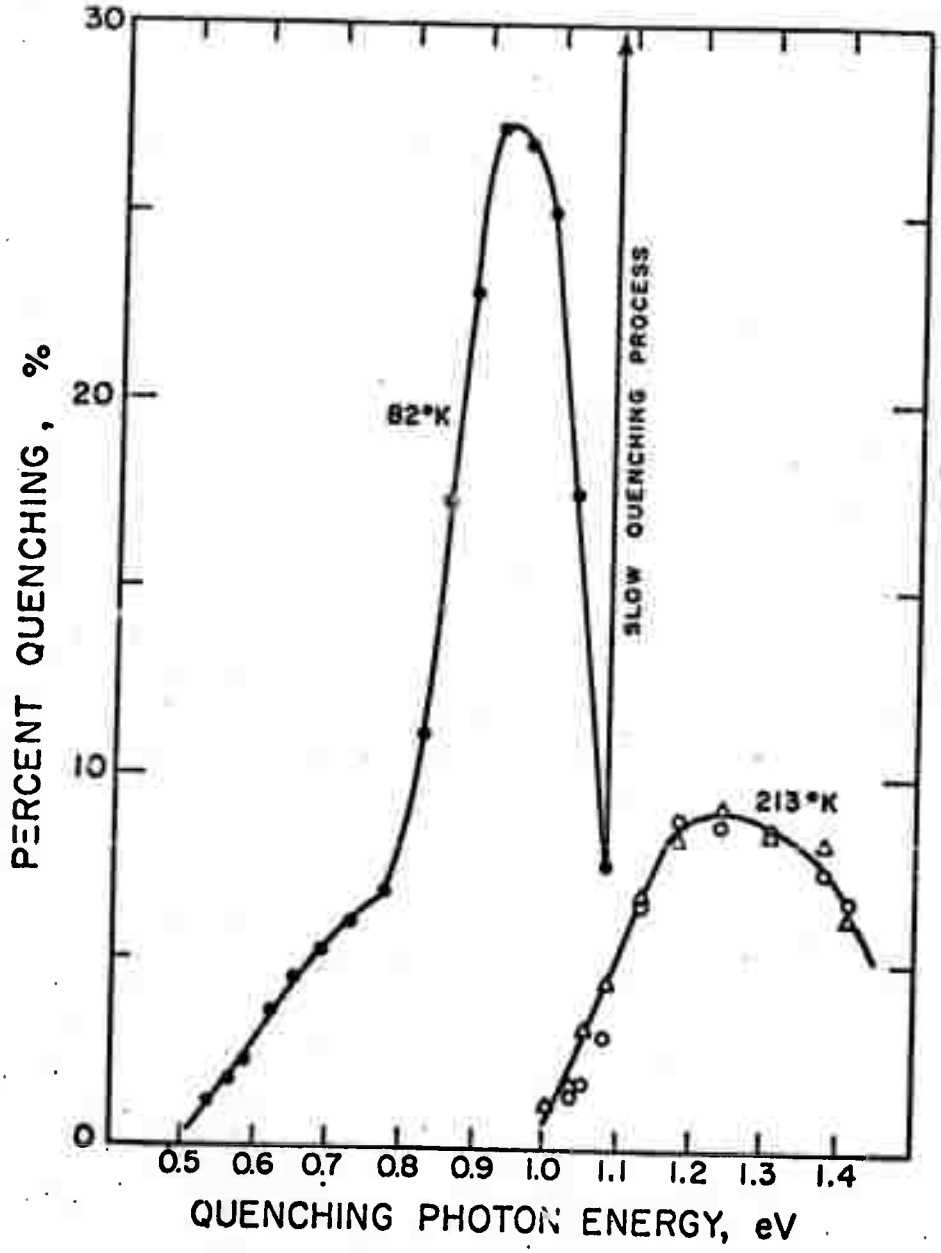

Figure 10. Optical quenching spectra for GaAs:O crystal at 213°K and at 80°K. The data at 213°K are for two different relative quenching intensities of 1 (▲) and 0.4 (o). f = 1 corresponds to 3.5×10^{13} photons cm^{-2} sec^{-1}.

V. SCIENTIFIC ASPECTS OF GALLIUM ARSENIDE CRYSTAL PREPARATION

W. A. Tiller and Hyo-Sup Kim

A. PROGRAM OBJECTIVES

The objective of this investigation is to develop an understanding of the important interfacial parameters that govern the growth of GaAs crystals. The study includes both the structures and energies of the solid-liquid interface in the Ga-As system as a function of (i) the concentration of the liquidus solution (at the liquidus temperature) and (ii) the orientation of the GaAs crystal.

B. PROGRESS TO DATE AND PRESENT STATUS

Previously, methods and atomic potential functions have been evaluated to determine the structure and energetics of the solid-liquid interfaces. Recently, each step has been reexamined and the treatment refined to produce more satisfactory results. Thus far, atomic interaction energy functions for the Ga-As system and the quasi-chemical term of the interfacial energy have been recalculated.

1. Ga-As System Atomic Interaction Energy Functions

For the crystal, the energy functions for the short-range interactions have been determined by utilizing the parametric method with additional high temperature data. This allows the energy functions to be effective over the wide range of temperature of interest in this study. These short-range energy functions are given in Fig. 1 along with the satisfactory long-range functions previously determined. For the liquid solution, average energy functions, utilizing new data, have been determined as a function of solution concentration using the earlier method.

These energy functions show a satisfying consistency over the temperature range of our interest and have been tabulated in Table 1. Using the Berthelot rule, the energy functions for the solid-liquid interaction are presented in Table 2.

2. Quasi-Chemical Contribution

Using these recalculated energy functions, the previously described quasi-chemical interaction term has been calculated for various temperatures and liquid concentrations. The lattice summation method was used in the evaluation of both the solid-solid and liquid-liquid interactions whereas the layer summation method was used for the solid-liquid interaction.

The excess energies contribution by the partial and total liquid-liquid interactions are tabulated in Table 3 to show the relative magnitude of the energies associated with the 1st, 2nd and total layer interaction. For the solid-solid interaction, the excess energies, E_s^x, are plotted as a function of temperature in Fig. 2. In addition, the quasi-chemical contributions to the excess energy of formation, E_{SL}^{ox}, of the unrelaxed planar interface are shown in Fig. 3. From Fig. 3, we can see that both the anisotropic features and the temperature dependence are similar to E_S^x. The broken line in the figure indicates an approximated E_{SL}^{ox} for the (100)/liquid interface with atomic roughness such that polarity has disappeared.

C. FUTURE WORK

The relaxation contributions will be considered to determine both the alterations in interface structure and energetics. The effect of

these characteristics on various interface kinetic phenomena will also be considered.

TABLE 1

Parameters for Interaction Energy Functions for the Liquid Solution

X_{As}	ϕ^o (e.v./pair atoms)	α ($Å^{-1}$)	r^o (Å)
0.0	0.243082	0.988345	3.324193
0.1	0.198510	0.857391	3.503222
0.2	0.174017	0.780843	3.618023
0.3	0.162120	0.741851	3.670777
0.4	0.154246	0.715509	3.692541
0.5	0.155513	0.719720	3.656621
0.6	0.164616	0.748866	3.576020
0.7	0.183399	0.804073	3.459383
0.8	0.213472	0.883055	3.332259
0.9	0.245415	0.952178	3.260614
1.0	0.265823	0.984998	3.290376

TABLE 9

Parameters for Interatomic Interaction Energy Functions for the Attractive Interactions between the Solid and the Liquid Phases Across the Interface. $\epsilon(r) = \sum_{i=1,2,3} \phi_i^o \exp(-\alpha_i(r-r^o))$

(a) For the interaction between a Ga atom in the solid and an average liquid atom.

		X_{As}					
	i	0.00	0.10	0.20	0.30	0.40	0.50
ϕ_i^o	1	-0.003717398	-0.005126424	-0.006159748	-0.006991486	-0.007831066	-0.008636705
	2	-0.05757658	-0.07818716	-0.09202694	-0.1035133	-0.1136817	-0.1247479
	3	-0.04432459	-0.05849307	-0.06697833	-0.0745263	-0.08028972	-0.08800572
α_i	1	4.093893	4.004368	3.946573	3.920937	3.896733	3.900461
	2	2.051195	1.968882	1.916948	1.892969	1.872186	1.87541
	3	1.011561	0.9385961	0.8942768	0.8726997	0.8562121	0.8588131
r^o		2.51392	2.52177	2.52421	2.52362	2.52113	2.51758

TABLE 2
(continued)

(Cont. of (a))

	i	X_{As} 0.60	0.70	0.80	0.90	1.00
ϕ_i^o	1	-0.00952484	-0.01045398	-0.01155612	-0.01264144	-0.01366594
	2	-0.1376042	-0.1529138	-0.1719618	-0.1920325	-0.2114855
	3	-0.09773522	-0.1110178	-0.1282976	-0.1469253	-0.1636117
α_i	1	3.922311	3.968390	4.030448	4.083494	4.100538
	2	1.895119	1.935525	1.990568	2.037792	2.054899
	3	0.8756839	0.9088968	0.9551869	0.9952527	1.012084
r^o		2.51300	2.50712	2.50101	2.49925	2.50807

Table 2
(continued)

(b) For the Interaction between an As atom in the solid and an average liquid atom.

	i	X_{As} 0.00	0.10	0.20	0.30	0.40	0.50
σ_i^o	1	-0.01296877	-0.01885883	-0.02251591	-0.02583321	-0.02849629	-0.03179456
	2	-0.2033526	-0.2849228	-0.3363867	-0.3803689	-0.4165667	-0.4589685
	3	-0.1584811	-0.2111114	-0.2448300	-0.2723199	-0.2963370	-0.3236109
α_i	1	4.103104	3.997385	3.946566	3.916888	3.901849	3.900038
	2	2.057168	1.964285	1.9169538	1.890307	1.875580	1.875151
	3	1.014014	0.9366909	0.8942797	0.8715997	0.8576219	0.8587037
r^o		2.51392	2.52177	2.52421	2.52362	2.52113	2.51758

Table 2
(continued)

(Cont. of (b))

	i	X_{As} 0.60	0.70	0.80	0.90	1.00
ϕ_i^o	1	-0.0350720	-0.03881473	-0.04269896	-0.04648674	-0.05040377
	2	-0.5066123	-0.5645304	-0.6342390	-0.7075986	-0.7800678
	3	-0.3598203	-0.4075093	-0.4723813	-0.5423859	-0.6035047
α_i	1	3.922223	3.964182	4.029113	4.084974	4.100582
	2	1.895097	1.932771	1.989725	2.038718	2.054919
	3	0.8756793	0.9077612	0.9548444	0.9956193	1.012091
r^o		2.51300	2.50712	2.50101	2.49925	2.50807

Table 3

Excess Energy Contributed by the Liquid-Liquid Interactions

Liquidus		E^x_{L1} (erg/cm)	E^x_{L2} (erg/cm)	E^x_L (erg/cm)
X_{As}	T(°K)			
0.025	1080	1701.9	631.3	2333.2
0.050	1154	1688.7	677.0	2365.7
0.100	1244	1642.7	747.2	2389.9
0.200	1365	1602.7	853.2	2455.9
0.300	1443	1590.3	919.7	2510.1
0.400	1494	1570.2	941.7	2511.9
0.500	1511	1581.2	938.2	2519.3

FIGURE CAPTIONS

Figure V-1. Atomic interaction energy functions for the GaAs crystal.

Figure V-2. The excess energies contributed by the solid-solid interactions.

Figure V-3. The quasi-chemical terms for the unrelaxed solid-liquid interface.

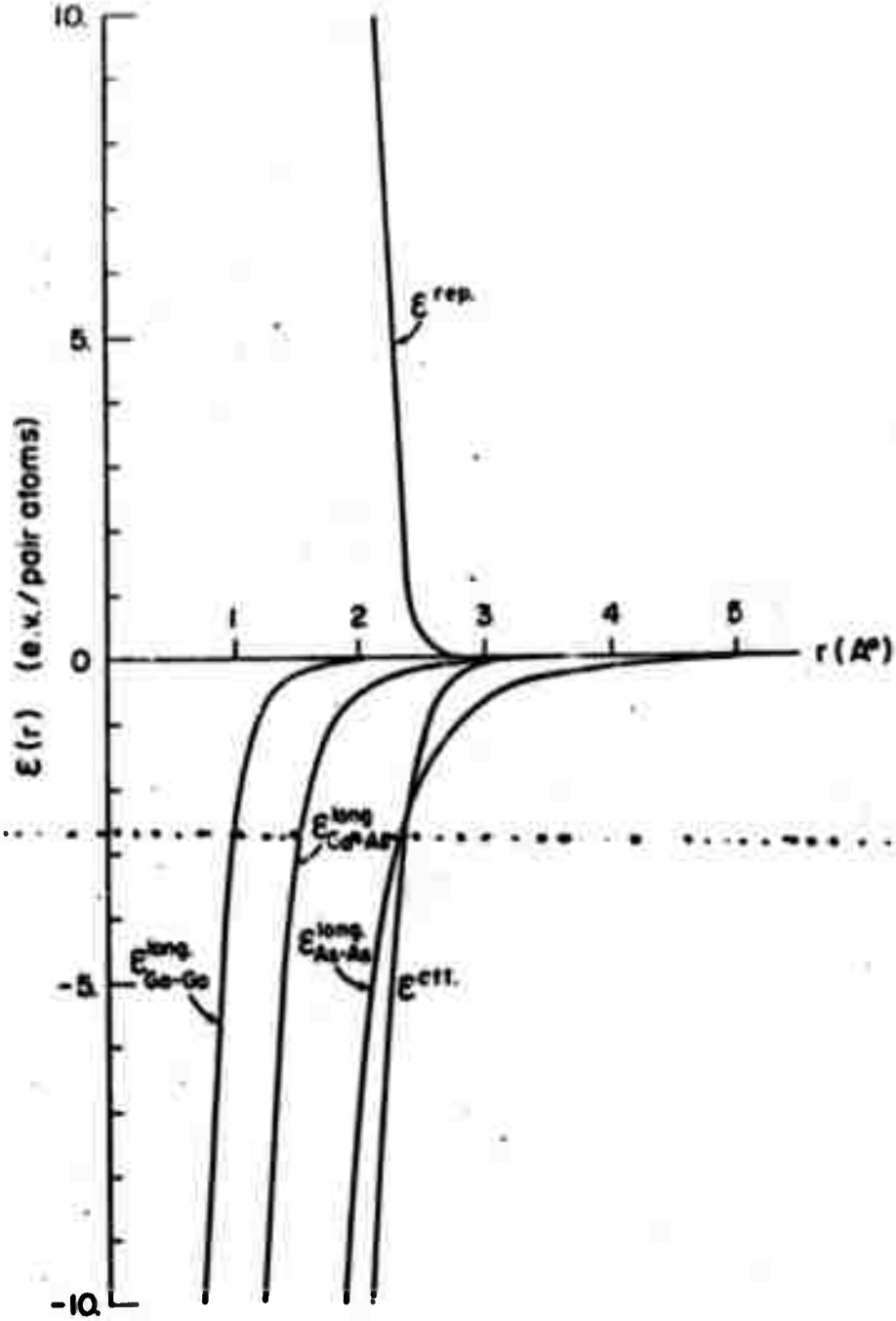

Figure V-1. Atomic interaction energy functions for the GaAs crystal.

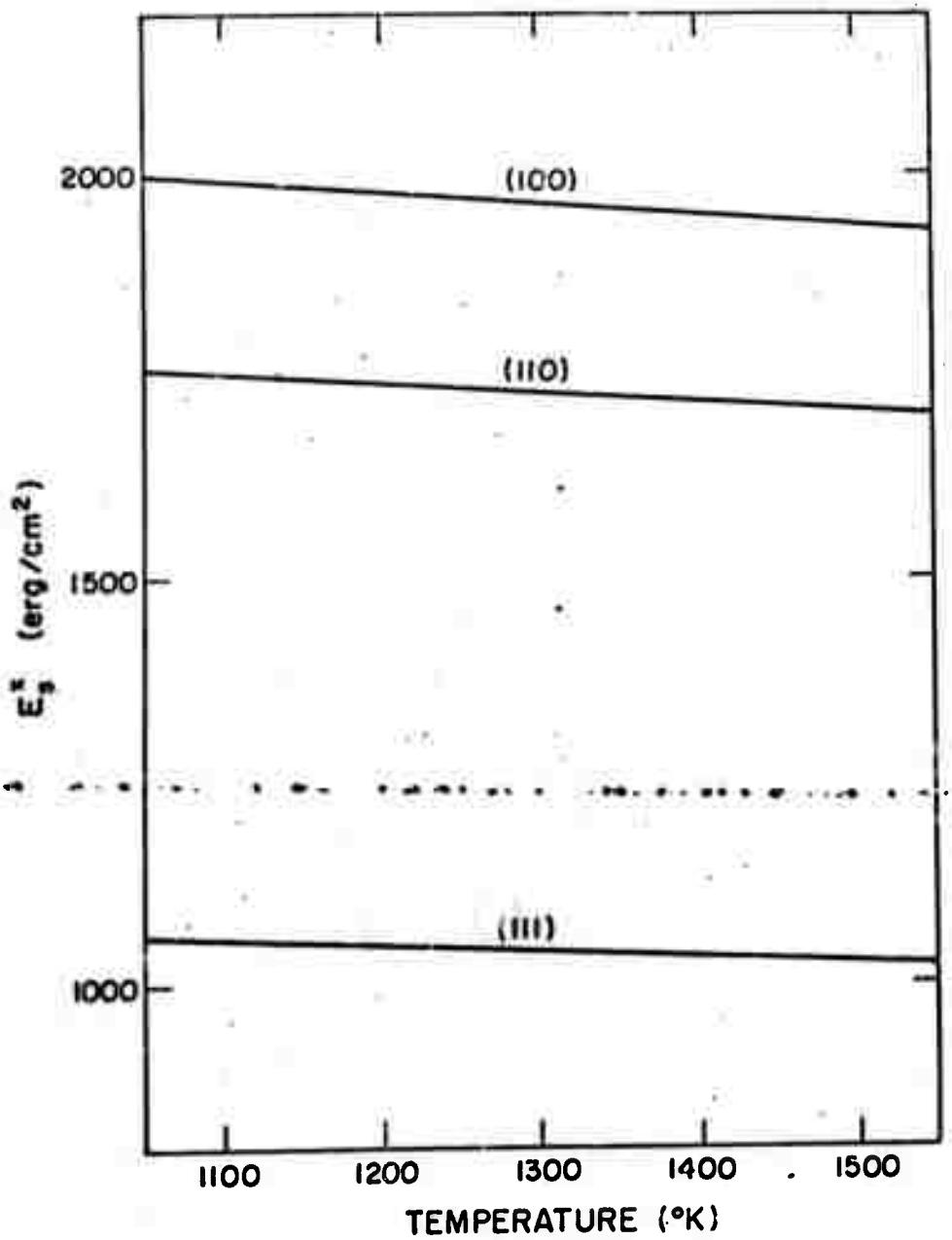

Figure V-2 The excess energies contributed by the solid-solid interactions.

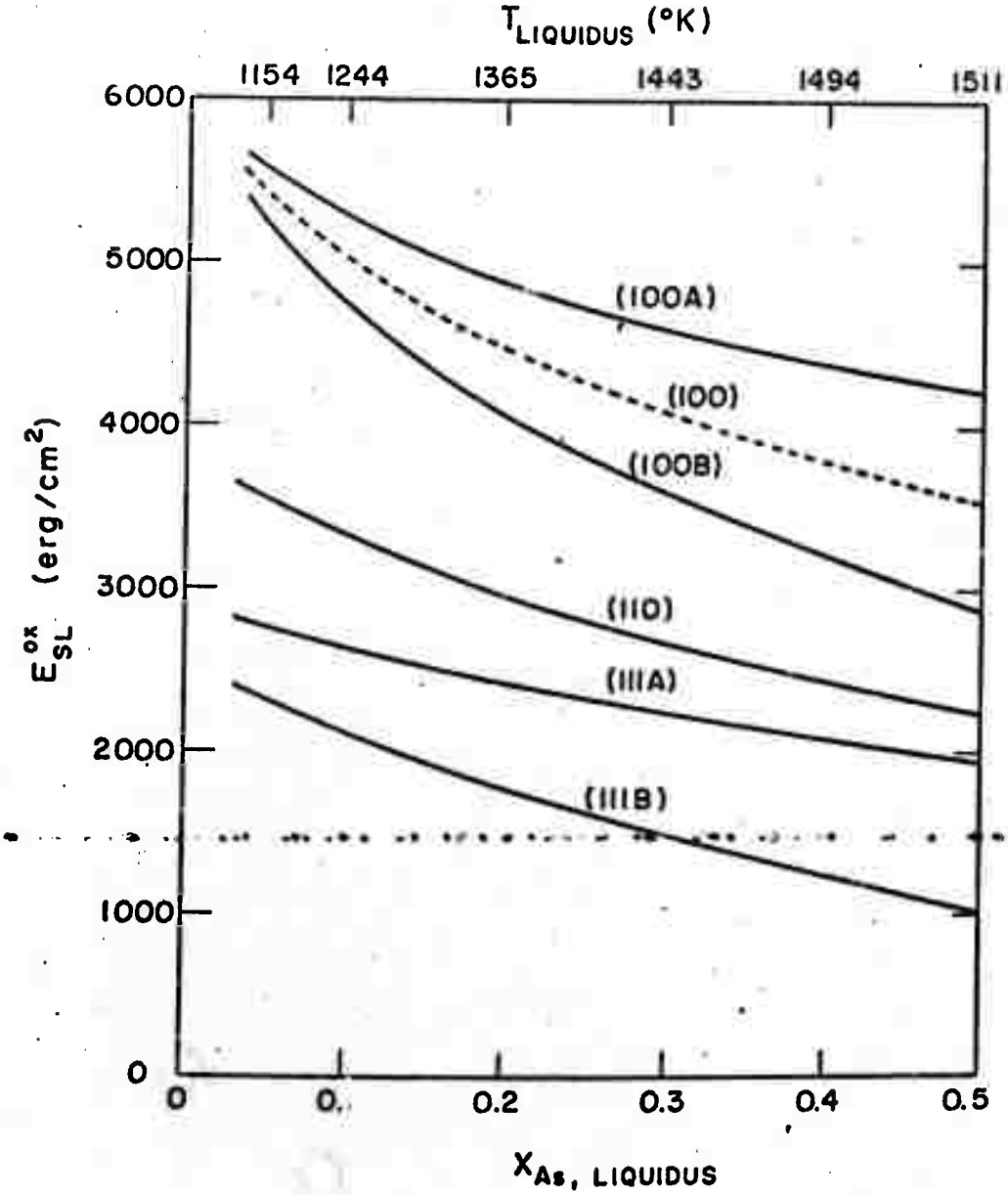

Figure V-3. The quasi-chemical terms for the unrelaxed solid-liquid interface.

VI. VAPOR PHASE GROWTH OF GaN ELECTROLUMINESCENT DIODES

D. A. Stevenson and H. P. Maruska

A. PROGRAM OBJECTIVES

As mentioned in previous reports, GaN and AℓN have recently attracted interest for their luminescent properties and piezoelectric properties, respectively. The objective of this program was to study the influence of growth parameters on the properties of these materials, with particular reference to their application to devices. During the period covered by this report, a structure was synthesized in GaN from which violet light emitting diode devices were fabricated. Owing to the novelty and potential of such devices, a major effort is being devoted to this topic.

Other workers have fabricated light emitting-diodes (LED's) from GaN that emit green and blue light. The structure utilized is an i-n junction, where the n-layer is undoped (but contains more than 10^{18} electrons cm^{-3}, probably due to a native donor defect) and the i-layer (intrinsic layer) is achieved by doping with Zn during growth. The Zn apparently forms a complex with the native donor, and then acts as a deep acceptor level.

No device has yet been shown to be capable of producing useful electroluminescence in the high energy (violet) end of the visible spectrum. Since GaN has a band gap of 3.5 eV, one may presume that the incorporation of an acceptor at less than 0.5 eV above the valence band would produce light in this short wave-length region. In this quest for such an acceptor, we have synthesized GaN with Mg doping additions. This dopent does indeed produce insulating materials, which have been synthesized as a layer on undoped GaN to produce the basic structure for the violet light emitting diodes.

B. PROGRESS

Single crystal epitaxial GaN layers were grown by the open flow vapor growth process previously described. Gallium is transported as its gaseous monochloride and the nitrogen is introduced into the growth zone in the form of ammonia. Substrates were held at a temperature of 925°C. The apparatus was modified to allow dopants to be introduced. This was done by adding a quartz sidearm tube perpendicular to the main growth tube, in the region of the center furnace zone, and just upstream of the ammonia outlet. The sidearm was equipped with its own furnace. A graphite crucible containing the proposed dopant in its elemental form is lowered in the sidearm into the furnace region, where it either forms a vapor for transport into the main tube, or else a chloride vapor is formed by passing HCl over the element. Doping is readily initiated or terminated by raising or lowering the crucible.

1. Zn Doping.

Several layers of Zn-doped GaN were grown on sapphire substrates. No change in sample properties except color (which became gradually more orange) was found with increasing crucible temperature until a critical Zn vapor pressure was achieved, at which point the samples became high-resistivity. This Zn vapor pressure was 10 Torr (the top of the crucible was held at 600°C).

Point-contact diodes were made as follows: two wires were positioned on the surface of a sample, consisting of an i-layer on top of an n-layer, with micromanipulators. A high voltage was then applied, causing a burning through to the highly conducting n-layer. This resulted in ohmic contacts. One contact was then repositioned, and about +80 volts applied to it.

Rectifying characteristics were then obtained and green light characteristic of Zn-doping in GaN could be seen.

2. Mg-Doping

Mg-doping was achieved by replacing the Zn in the crucible with Mg and inserting it to the 720°C position in the furnace, where the Mg vapor pressure is 10 Torr. These samples were light yellow in color and highly resistive. Point contacts fashioned as described above gave violet light, which peaked at 2.92 eV with 160 volts applied. The light was just visible in a well-lit room if the viewer cast a shadow upon the sample with his hand. As far as we are aware, this is the first report of electroluminescence, visible to the eye, at this short wavelength.

3. Light-emitting-diodes in GaN:Mg

By varying some growth parameters and by developing a contacting procedure, it was possible to obtain violet LED's which operated at low voltages. After the growth of an undoped n-type region for 30 mins (about 10μ thick), the Mg crucible is lowered for 6 mins. Then it is raised again, and the growth continued for 7 more minutes. The final layer is not conducting, because the system apparently has a memory for the dopant. However, the doping level is decreased toward the surface, and this facilitates contacting. Without the terminal layer, it is not possible to make a large area contact.

Contacts to the n and i regions are made with an indium amalgam (90% In-10% Hg). This amalgam is a liquid at room temperature, and is painted onto one edge to form an ohmic contact to the n region and onto the face of the insulating region. The chip is then heated for 1 min at 400°C to drive off the mercury, leaving solid indium contacts. The

devices were then either glued to glass slides with glycol-phthalate (sapphire to glass) or mounted on TO-15 transistor headers (sapphire up, see Fig. 1). Light is emitted from the area under the contact to the i-region, which can be as large as 2mm x 2mm.

Electroluminescence was obtained both with "forward" (i-layer biased positive) and "reverse" bias, although the forward bias luminescence was more efficient. In the forward direction, substantial conduction began at about 10 volts, and violet light, readily seen in a well-lit room, was obtained at 20 volts. Under reverse bias, conduction occurred in the 40-60 volt range and produced green light. Emission under forward bias electroluminescence peaked in the region of 2.86 to 2.98 eV in various samples. The spectral width at half-maximum is about 400 meV. A typical spectrum is shown in Fig. 2. The peak has been found to shift to shorter wavelengths with increasing current until a saturation value is reached. An example of this effect is shown in Fig. 3. The light output increases superlinearly with current but linearly with power input. In reverse bias, a broad peak centered at 2.5 eV and about 750 meV wide at half maximum is obtained. This is shown in Fig. 4. We do not as yet understand the shift in emission wavelength from forward to reverse bias.

The I-V characteristic of a typical device is displayed in Fig. 5a. The current drawn by a particular sample is dependent on the contact area, but since the emitted light shows a very nonuniform pattern, it is not possible to ascertain the current density. A log-log plot of the current-voltage characteristics is shown in Fig. 5b. With forward bias, I is proportional to V^3 in the region $10 < V < 30$ where the violet light is emitted. A steeper dependence is found at smaller voltages. At a given voltage the reverse current is about two order of magnitude smaller.

The power efficiency increases with increased forward bias up to 15 V, beyond which it is nearly constant at a value of 10^{-5}. The reverse bias efficiency is an order of magnitude lower (see Fig. 6). The diodes operate continuously at room temperature.

Photoluminescence of Mg-doped GaN was excited with a He-Cd laser which emits at 3250Å, and the resulting spectrum was found to peak at 2.925 eV at 77°K (Fig. 7). This indicates that the Mg complex forms a level about 0.5 eV above the valence band in GaN. It has been suggested by workers at Bell Telephone Labs that Zn first forms a shallow acceptor level when present in small quantities and with increased doping results in a deep Zn-donor complex, which compensates the native donors present and is responsible then for the resistivity increase and sample color changes which are observed. It is reasonable to assume that the same process holds for Mg doping. Although the photoluminescent results were obtained at 77°K, one may expect that there will be no shift in this spectrum in going to room temperature. Thus the forward bias electroluminescence at 300°K corresponds well to the photoluminescent data, and the same level is apparently involved.

The foregoing results show that it is possible to obtain electroluminescence in Mg-doped GaN diodes which require about 20 volts for operation and which can emit at shorter wavelengths than Zn-doped GaN diodes. A power efficiency similar to that found in the Zn-doped blue-emitting diodes is found, and the luminescence is readily seen in a well-lit room, in spite of the eye's decreased sensitivity in the violet region of the spectrum. The $I \propto V^3$ characteristic is suggestive of space charge limited current in the presence of an exponential distribution of the

traps. An exponential distribution of traps is consistent with the shift of the light emission peak to shorter wavelengths with increased input current. Assuming that the traps are being emptied by field emission, then levels nearer the valence band (which will have a greater density) will be emptied at higher applied fields. However, a maximum in the distribution of traps must be assumed to explain the saturation when the traps of maximum density are being emptied.

4. Ion Implantation

There are no successful reports in the literature of diffusion in GaN. Conventional techniques, such as heating a sample in Zn vapor, have not yielded any results. It has been possible recently to assist diffusion by bombarding a material with protons. This method has met with success in Si and Ge. An undoped wafer of GaN was coated with a 500Å layer of Zn, and masked over with Si_3N_4 to prevent evaporation. The sample was then bombarded for 5 hours with a proton current of 1μA, while heated to a temperature of 600°C. The Si_3N_4 and residual Zn were then removed in HF. The sample surface now proved to be highly resistive and lightly orange colored. It had been held in place during the diffusion with a tungsten clip, and the shadow of the clip was plainly visible. The region masked by the tungsten maintained its normal low resistance.

Several indium contacts were made to this sample. They showed rectification, and visible yellow-green light was emitted from one of these contacts. However, it burned out before the spectrum could be measured.

An electron microprobe analysis failed to show the presence of Zn in the sample. However, about 3×10^{19} Zn atoms cm^{-3} would have had to

have been present for their presence to have been above the detection limit, so the results are inconclusive.

C. PLANS FOR FUTURE WORK

Work is continuing in an effort to elucidate the mechanism responsible to the electroluminescence in the GaN:Mg diodes. This includes studies of the wafer surfaces with the scanning electron microscope and the bulk of the crystals with the transmission electron microscope. Variations in growth times and temperatures and in dopant concentrations are also being studied in order to maximize light output efficiencies. Also, the effect of substrate orientation is under study.

FIGURE CAPTIONS

Figure VI-1. Schematic diagram of the GaN:Mg electroluminescent diode.

Figure VI-2. Electroluminescent spectrum with forward bias.

Figure VI-3. Shift of forward-bias electroluminescence peak with input current.

Figure VI-4. Electroluminescent spectrum with reverse bias.

Figure VI-5a. Typical I-V characteristic.

Figure VI-5b. Log-log plot of current-voltage characteristic.

Figure VI-6. Power efficiency.

Figure VI-7. Photoluminescence spectrum at 77°K.

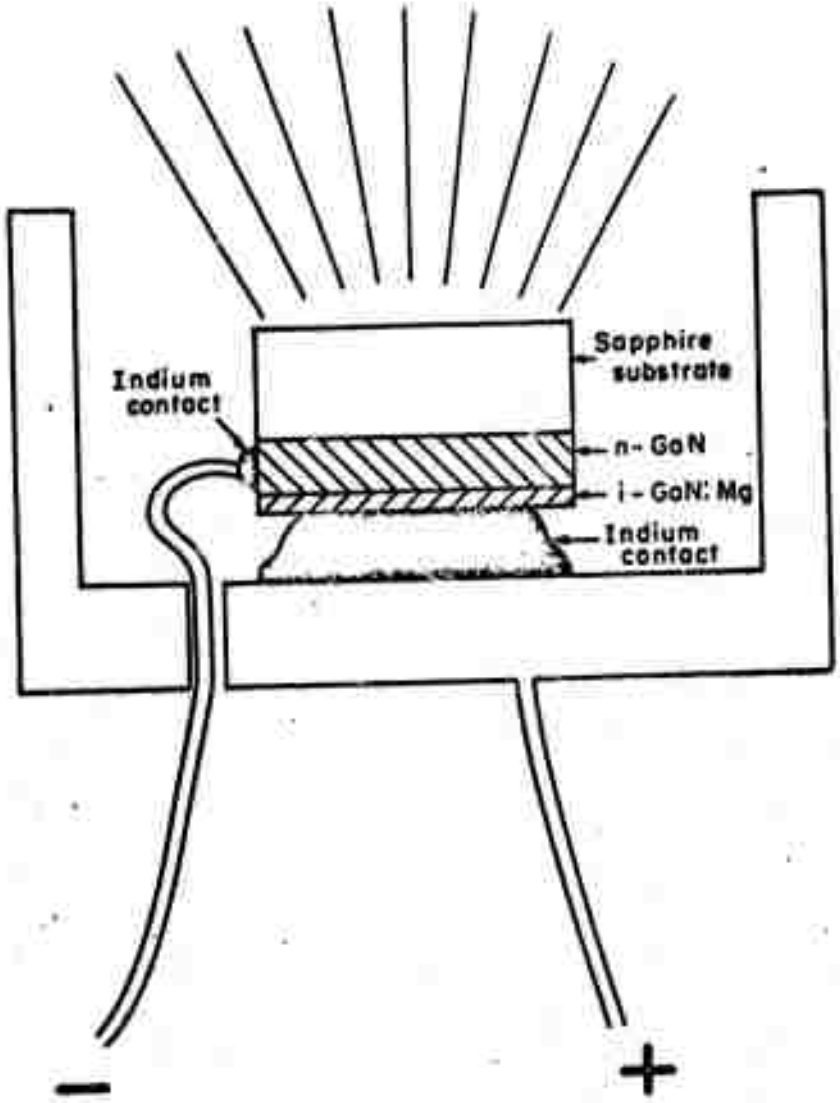

Figure VI-1. Schematic diagram of the GaN:Mg electroluminescent diode.

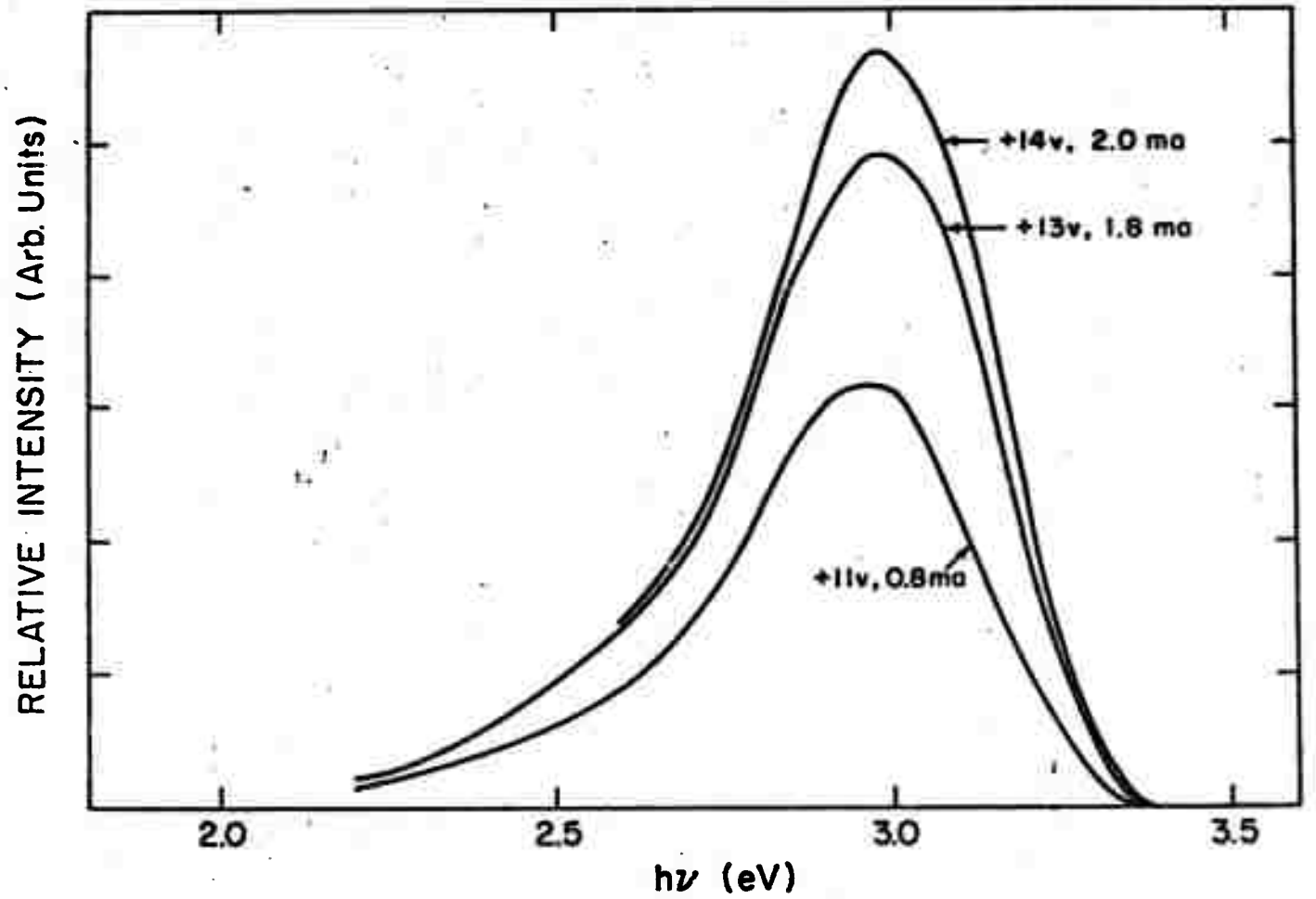

Figure VI-2. Electroluminescent spectrum with forward bias.

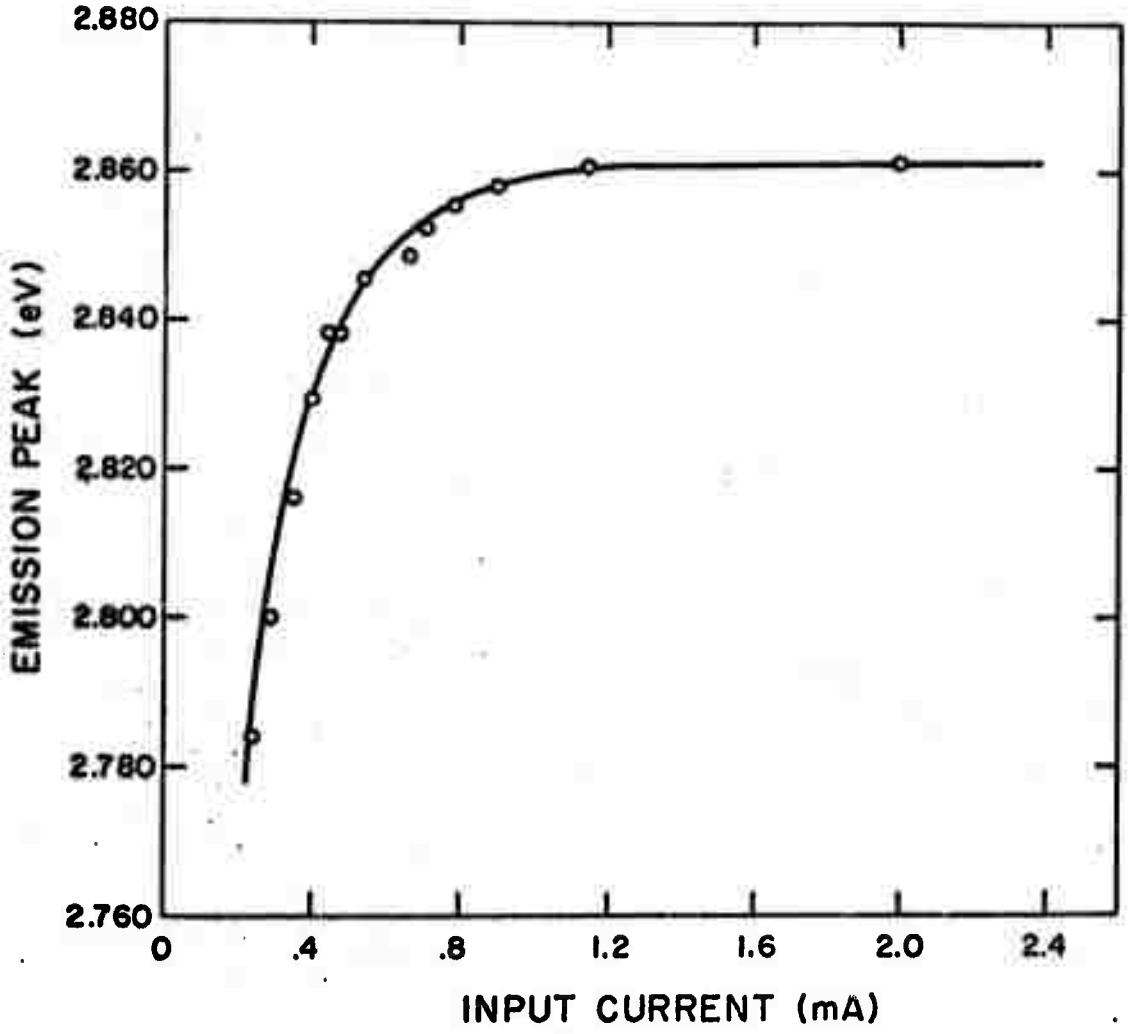

Figure VI-[illegible]. Shift of forward-bias electroluminescence peak with input current.

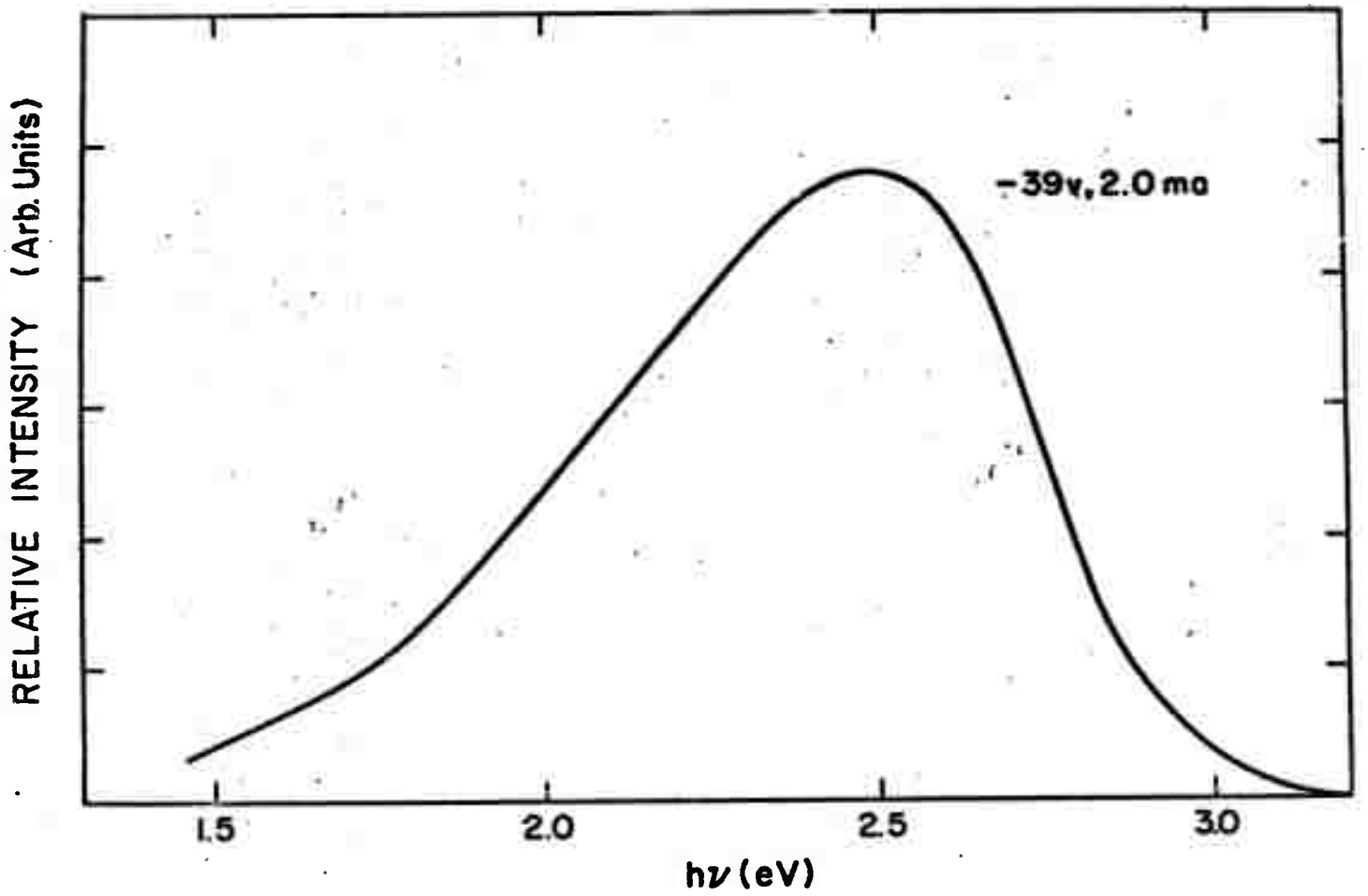

Figure VI-4. Electroluminescent spectrum with reverse bias.

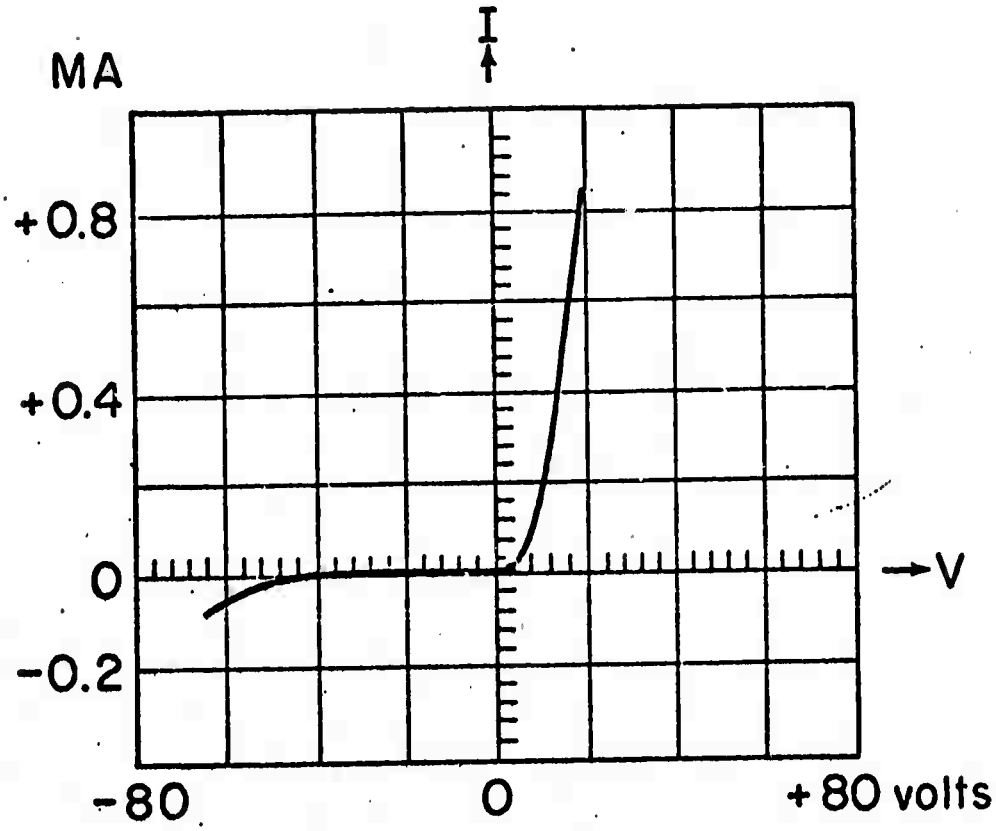

Figure VI-5a. Typical I-V characteristic.

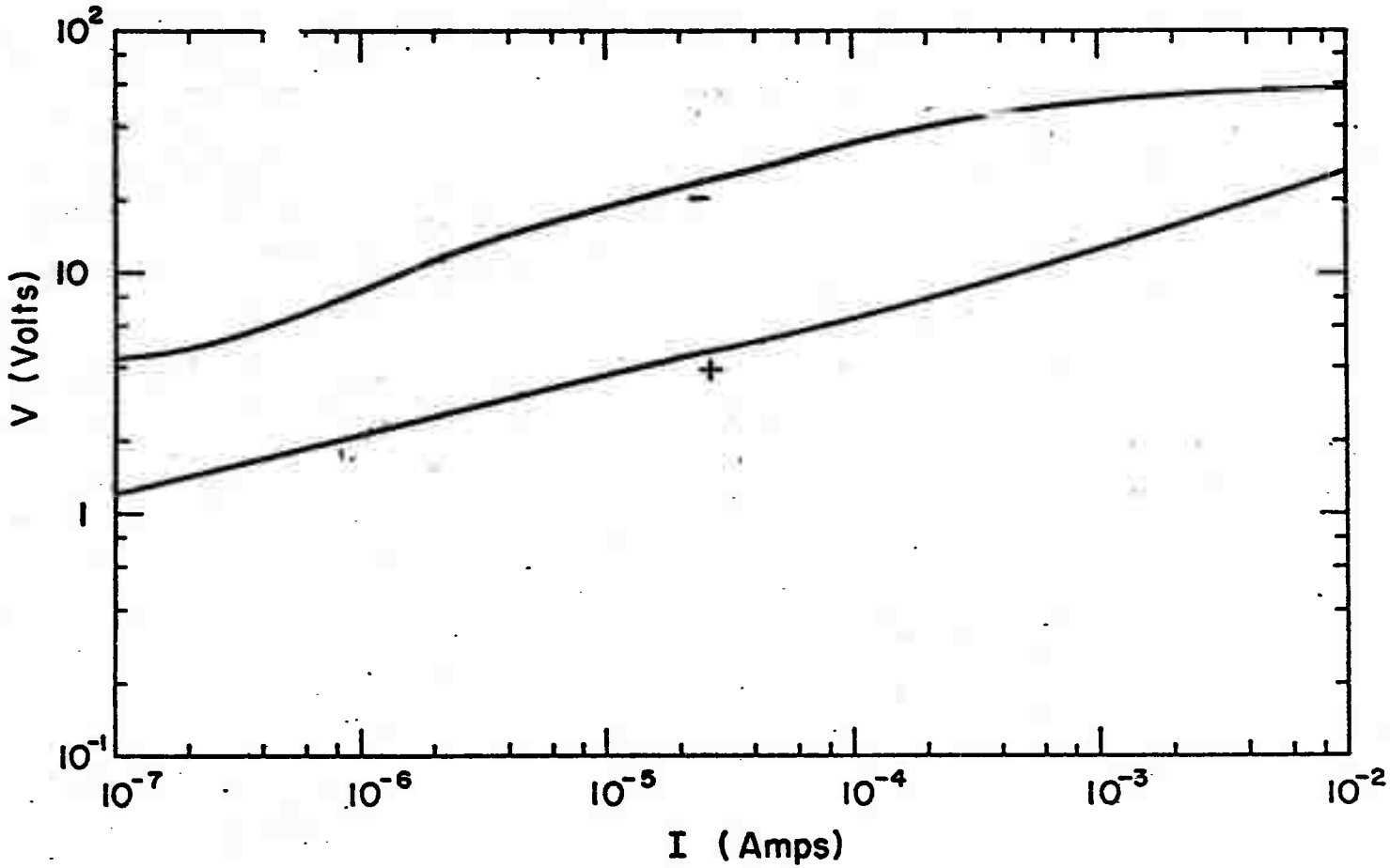

Figure VI-5b. Log-log plot of current-voltage characteristic.

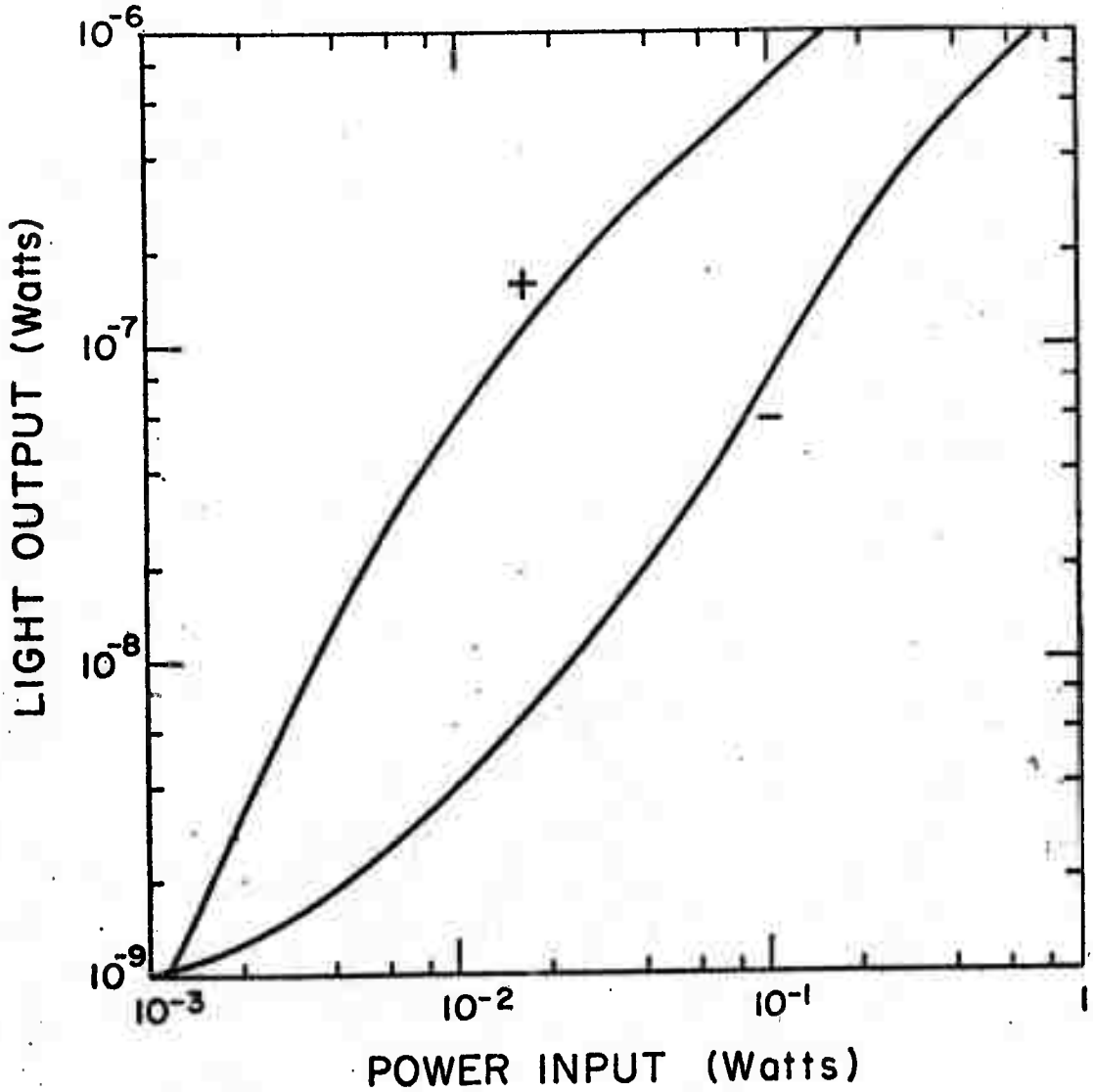

Figure VI-6. Power efficiency.

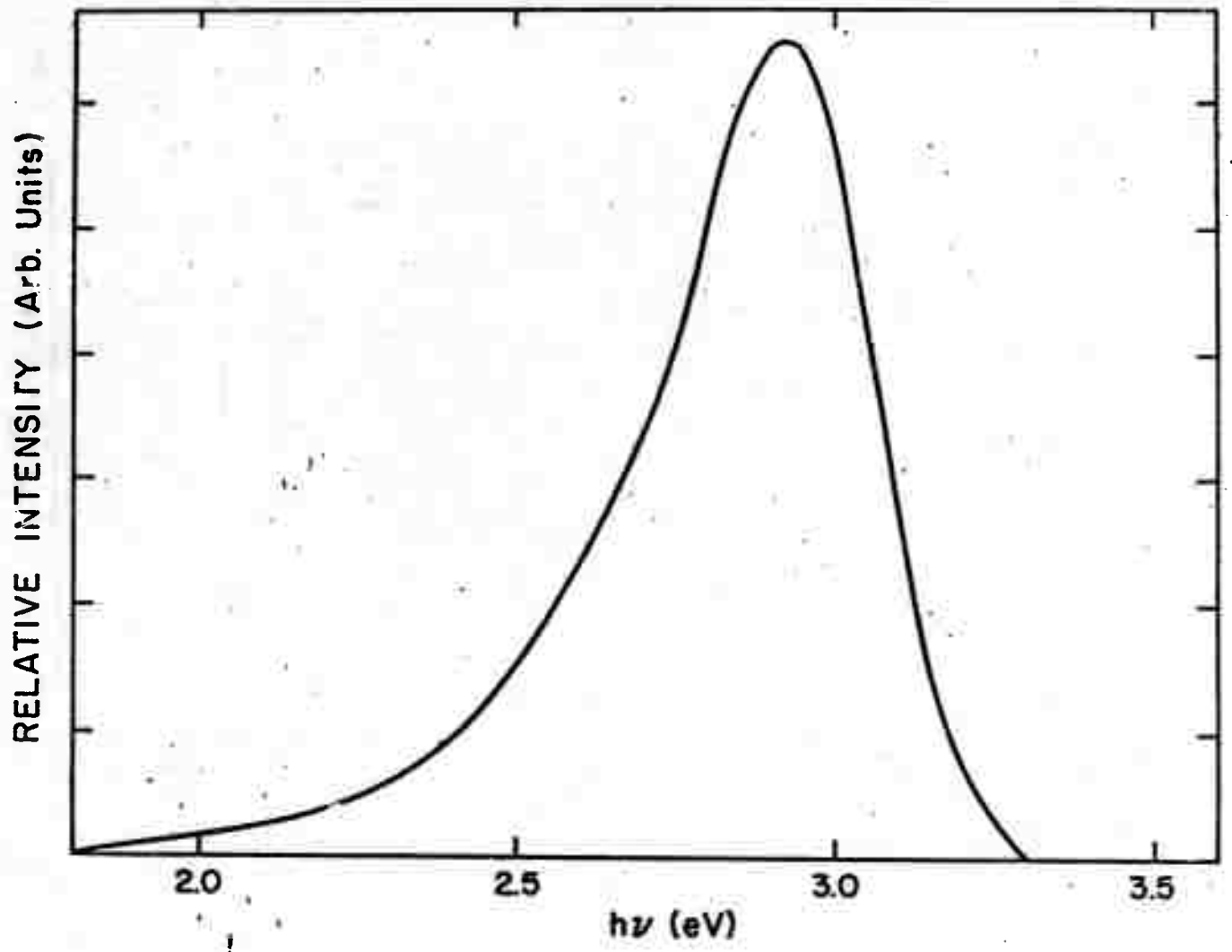

Figure VI-7. Photoluminescence spectrum at 77°K.